

# **Anchorage and Lapping of Reinforcement Steel Bars Under Fire**

## **Design Situation**



# **POLITECNICO MILANO 1863**

A thesis in partial fulfilment of the requirements for the degree of

**Master of Civil Engineering**

by

Mehtab Qamar

in supervision of

Prof. Giovanni Muciaccia

School of Civil and Environmental Engineering

Faculty of Engineering

Academic Year 2018-2019



# ACKNOWLEDGEMENTS

In the first place, I would like to thank the Almighty God to bless me with an opportunity to pursue the academic path I wished for. Secondly, I would like to express my sincere gratitude to Prof. Giovanni Muciaccia for guiding me, sparing his valuable time, suggestions and continuous follow up to keep me in right direction to achieve the desired goals.

I would like to also thank my parents for their continuous support in all fields of my life, for inspiring me and motivating me through ups and downs, my siblings and my friends and colleagues who are constant source of encouragement for me with their influential personality and behavior with me.

Last but not the least, I would also like to thank Politecnico Di Milano and its academic and organizational staff for humble dealing in all aspects with international students and for providing me one of the life time chance to pursue higher education here that I had wished once.

# Contents

Chapter 1 .....	9
Introduction.....	9
1.1 Background .....	9
1.2 Research Objectives.....	11
1.3 Thesis Outline .....	12
Chapter 2.....	13
Literature Review.....	13
2.1 Introduction.....	13
2.2 Mechanism of bond transfer between reinforcement and concrete.....	15
2.3 Factors influencing bond stresses and anchorage of reinforcement.....	20
2.4 Fundamental theories and factors for anchorage and bond in RC members.....	21
2.4.1 Bar stress - Semi-empirical expression .....	22
2.4.2 Basic bond strength.....	24
2.4.3 Design bond strength .....	25
2.4.4 Design anchorage length.....	27
2.5 Eurocode 2 .....	27
2.6 Effect of Elevated Temperature on Concrete Properties.....	29
2.6.1 Concrete Compressive Strength.....	29
2.6.2 Concrete Tensile strength.....	31
2.6.3 Bond behavior at Elevated Temperature.....	31
Chapter 3.....	35
Analysis Methodology .....	35
3.1 Heat transfer analysis .....	35
3.1.1 Modelling parameters .....	35
3.1.2 Fire Modelling .....	38
3.1.3 Numerical Modelling .....	40
3.1.4 General Observations .....	41
3.2 Proposed scheme for incremented embedded length.....	44
3.2.1 Anchorage at beam-column connection.....	44
3.2.2 Laps.....	46
3.3 Amplification factor.....	47
Chapter 4.....	48

Results.....	48
4.1 Bond strength $f_{bd(T)}$ distribution.....	48
4.2 General observations.....	49
4.2.1 Pre-cast rebars.....	49
4.2.2 Post-Installed rebars.....	50
4.3 Amplification factor vs Bar diameter.....	51
4.4 Amplification factor vs concrete cover.....	54
4.5 Amplification factor for Laps.....	65
Conclusion.....	66
References:.....	69
Annex A.....	73
MATLAB CODE:.....	73
Annex -B.....	78
Temperature Data.....	78
Annex-C (Example Calculation).....	88

# List of Figures

Figure 2.0.1 Typical cases in hand (a)anchorage (b) laps.....	14
Figure 2.2 Mechanism of bond transfer in reinforced concrete (Wight and Mecgregor 2012) .....	16
Figure 2.3 Stages of bond resistance in typical bond stress-slip law .....	16
Figure 2.4 Splitting in reinforced concrete: (a) typical stress peaks; (b) bar-concrete slip and wedging action; (c) main parameters.....	18
Figure 2.5 Modes of failure: (a) pull-out; (b) splitting-induced pull-out; (c) splitting accompanied by slip.....	20
Figure 2.6 Anchorage bond in tension bars .....	21
Figure 2.7 Definition of concrete covers.....	24
Figure 2.8 Values of K for different bar position .....	28
Figure 2.9 Compressive Load Behavior of normal strength concrete at elevated temperature .....	30
Figure 2.10 Details of specimen .....	32
Figure 2.11 Reduction Curves for pre-cast and post-Installed rebars (Muciaccia ).....	34
Figure 3.1 Investigated cases: (a) anchorage at beam-column node; (b) lap splice.....	35
Figure 3.3 Conductive Boundary condition for exposed surface.....	37
Table 3.3 Boundary condition for unheated surface .....	38
Figure 3.6 Standard fire curve ISO 834-1 .....	39
Figure 3.7 Fire curve input as amplitude .....	39
Figure 3.8 Sample meshed element .....	40
Figure 3.9 Temperature profile for time 120 minute .....	41
Figure 3.10 Temperature distribution at time R120 for different edge distances at beam-column connection.....	41
Figure 3.11 Temperature Path selection .....	42
Figure 3.12 Temperature gradient at 30 mm edge distance .....	43
Figure 3.13 Temperature gradient for time 120 minute.....	43
Figure 3.14 Anchorage at beam-column node, example of temperature distribution along the bar .....	44
Figure 3.15 Bond strength distribution along the bar .....	46
Figure 3.16 Demonstration of laps in a slab .....	47
Figure 4.1 Bond strength distribution along the rebar length for pre-cast side .....	48
Figure 4.2 Bond strength distribution at different edge distance (Y).....	49
Figure 4.3 Geometry of the transversal section of the specimens.....	50
Figure 4.4 Amplification factor pre-cast rebar, as a function of exposure time, rebar diameter $\phi 16$ and edge distance 80 mm.....	50
Figure 4.5 Amplification factor for pre-cast and post-installed rebars at edge distance 80 mm.....	51
Figure 4.6 Amplification factor for different diameters at 60 mm edge distance .....	52
Figure 4.7 Amplification factor for different diameters at 90 mm edge distance .....	52
Figure 4.8 Amplification factor for different diameters at 120 mm edge distance .....	53
Figure 4.9 Amplification factor for precast-side rebars at exposure time R30 .....	54
Figure 4.10 Amplification factor for precast-edge rebars at exposure time R30.....	55
Figure 4.11 Amplification factor for precast-center rebars at exposure time R30.....	56
Figure 4.12 Amplification factor for precast-side rebars at exposure time R60 .....	57
Figure 4.13 Amplification factor for precast-edge rebars at exposure time R60.....	58
Figure 4.9 Amplification factor for precast-side rebars at exposure time R90 .....	59
Figure 4.10 Amplification factor for precast-edge rebars at exposure time R90.....	60

Figure 4.12 Amplification factor for precast-center rebars at exposure time R90.....	61
Figure 4.13 Amplification factor for precast-side rebars at exposure time R120.....	62
Figure 4.14 Amplification factor for precast-edge rebars at exposure time R120.....	63
Figure 4.15 Amplification factor for precast-center rebars at exposure time R120.....	64
Figure 4.15 Amplification factor for laps .....	65

# List of Tables

Table 1. Specific Heat and Conductivity .....	36
Table 3.2 Surface radiation for exposed side .....	37
Table 3.3 Boundary condition for unheated surface .....	38
Table 4 Amplification factor for pre-cast side at edge distance of 60 mm .....	51
Table 5 Amplification factor for different diameters at 90 mm edge distance .....	52
Table 6 Amplification factor for different diameters at 120 mm edge distance .....	53
Table 7 Amplification values for different bar diameters at exposure time R30 .....	54
Table 8 Amplification factor for precast-edge rebars at exposure time R30 .....	55
Table 9 Amplification factor for precast-center rebars at exposure time R30 .....	55
Table 10 Amplification factor for precast-center rebars at exposure time R30 .....	56
Table 11 Amplification factor for precast-side rebars at exposure time R60 .....	57
Table 12 Amplification factor for precast-edge rebars at exposure time R60 .....	58
Table 13 Amplification factor for precast-side rebars at exposure time R90 .....	59
Table 14 Amplification factor for precast-edge rebars at exposure time R90 .....	60
Table 15 Amplification factor for precast-center rebars at exposure time R90 .....	61
Table 16 Amplification factor for precast-side rebars at exposure time R120 .....	62
Table 17 Amplification factor for precast-edge rebars at exposure time R120 .....	63
Table 18 Amplification factor for precast-center rebars at exposure time R120 .....	64

# Chapter 1

## Introduction

### 1.1 Background

Sufficient anchorage should be provided on both sides of critical sections in order to meet fundamental requirements of strength, ductility and robustness of a reinforced concrete (RC) structure. The anchorage on each side of a critical section must ensure that the tensile bars at the critical section not only develop the yield stress, but are also able to sustain it as the deformation increases. Therefore, codes of design (Eurocode 2-2004) specify a minimum length of anchorage for tensile bars, called the development length, over which a straight bar must be embedded in concrete in order to develop its yield stress.

Specified values of development length in the Eurocode 2-2004 have been developed independently as empirical fits to test results, obtained mostly from conventional bar pull-out tests. A pull-out test determines the average ultimate bond stress that develops in the short anchorage length of a bar when it is pulled out of a small RC specimen. The fundamental hypothesis that has been developed from the results of the pull-out tests is that if a bar has long enough embedment in concrete, the slip at the loaded end progresses far enough to develop bond over a considerable length (Ferguson, 1958). Such a bar cannot be pulled out; it rather fails in tension after reaching and sustaining the yield strength, and the minimum required length of anchorage to develop such a condition with an acceptable factor of safety is known as the development length.

The design provisions for the development length in the codes of practice are generally based on an estimated value of the average ultimate bond stress for the anchorage of a bar, which is directly related to the tensile strength of concrete and modified by coefficients of varying form and complexity to account for the factors affecting the bond strength. The tensile strength of concrete, as determined in a pull-out test, is a function of bar tension and bar length; and is not influenced by cracking caused by bending or external shear over the anchorage length similar to what may exist at the anchorage of a tensile bar in beam or slab in a RC structure. The average bond efficiency in real RC structures may be considerably worse, where loads can be repetitive and dynamic in nature, flexural cracks may occur across the anchorage length, shrinkage and temperature induced cracking can reduce the bond between concrete and steel, and where deterioration may occur due to the extensive periods of exposure to the elements.

While bond stresses are often uniform in the short anchorage length of a pull-out specimen, the bond stress in a typical RC flexural member is neither uniform nor uniformly varying from point to point (Ferguson, 1958). The conditions favorable for the development of (often) uniform bond stress in the pull-out tests are very rarely present in practical RC members, where the situation is more complex due to presence of adjacent bars developing stress and one or more cracks crossing the anchorage length. Different structural and material parameters variably influence the bond behavior in RC members.

Reinforced concrete structures are vulnerable to high temperature conditions such as those involved during exposure to fire. At elevated temperatures, mechanical properties of concrete and reinforcing steel as well as the bond between steel rebars and concrete may significantly deteriorate. The decrease in the bond strength may influence the stress carrying capacity of RC elements. Therefore, the assessment of bond strength degradation across the anchorage length and laps is required for structural design of fire safety. Consequently, there is a need to investigate the bond behavior between concrete and steel rebars when exposed to fire, and then

to propose a solution that accommodates the degradation effect. Specifically, the idea developed in current thesis work is to propose an amplification factor that can be multiplied with the basic anchorage length to find length increment depending on temperature and rebar position.

This thesis contains an analytical investigation on the residual bond strength between concrete and steel rebars across the embedded length after fire exposure. Also, it discusses the pre-cast and post-installed cases for different bar positions namely side, center and edge. Heat contours were found through FEM method for different geometrical cases such as beam-column connection, and laps. The analytical parameters considered in the current research include exposure condition, rebar type, rebar size, rebar location, and the presence of transversal stirrups.

## 1.2 Research Objectives

The main objective of this research is to assess the residual bond strength along the embedded length of rebar after the exposure to fire, and proposing a scheme that accommodates the damage by providing an amplification factor which then can be multiplied with basic anchorage length or lap length to get the incremented length:

1. Assess the post fire bond strength between steel rebars and concrete.
2. Investigate the effect of various parameters that affect residual bond strength after fire exposure such as; exposure conditions, concrete strength, rebar type, rebar size and rebar location.
3. Find length increment that come in result of damaged bond strength and propose an amplification factor that can be multiplied with basic anchorage length to design under fire situation.
4. Similarly, find amplification factor for different cases such as post-installed center, side, and edge, and for pre-cast laps; and compare the findings with previous results.

### 1.3 Thesis Outline

This thesis is organized according to the stages followed for the development of the investigation. Following is given a brief description for the chapters' contents:

- **Chapter (1):** Addresses the background, the scope and objectives of the research.
- **Chapter (2):** Includes a literature survey on behavior of bond between concrete and steel rebars at ambient temperature, the effect of elevated temperatures on reinforced concrete elements specifically for anchorage at beam-column connection, and laps. It also reviews different stages for evaluating bond behavior. At the end of this chapter, the research areas which are needed to be studied were identified.
- **Chapter (3):** The objectives, scope, and details of the analytical scheme is presented in this chapter. The details of the heat transfer analysis and bond reduction are also described.
- **Chapter (4):** Test results for the analytical work were presented in this chapter, with an analysis and discussion of the effect of various parameters.
- **Chapter (5):** Provides summary, conclusions, and recommendations for future work in the area of assessment and restoration of bond strength between concrete and steel rebars after fire exposure.

# Chapter 2

## Literature Review

### 2.1 Introduction

The success of reinforced concrete (RC) as a building material is largely due to the ability of reinforcement and concrete to act composite to withstand the structure's external loads and deformations. In order to efficiently work together concrete and reinforcing bars, the bar elements must be subjected to the same strain or deformation as the surrounding concrete to prevent potential discontinuity or separation of the two materials under load. Since external forces are rarely directly applied to the reinforcement (as they are in a pull - out specimen), the reinforcing bar can only receive its load share from the surrounding concrete (Park and Paulay, 1975; Fanella, 2011). For this interactive load transfer process to exist between the two materials, bond stresses must be applied along the bar - concrete interface to produce the necessary tensile or compressive stress change in a bar. Therefore, bond stresses are idealized as longitudinal shearing stresses acting in contact with the concrete along the circumferential contact surface of the bar. The bonding action, however, is needed not only to ensure an adequate level of safety by maintaining the composite action between the two materials, but also to control the structural behavior with adequate ductility and robustness.

For an RC member designed for strength, ductility and robustness, it is essential that the tensile bars in the critical section develop not only the yield stress of the reinforcement,  $\sigma_{y,f}$ , but also the stress level as deformation increases. Typical tensile bar anchorage conditions in a critical section of an RC member under bending are: (i) where a straight anchorage length ( $l_d$ ) is provided on both sides of the critical section; and (ii) where two adjacent bars are lapped in

such a way that the length of the lapped splice ( $l_s$ ) is sufficient to fully develop both bars. (see Figure 2.1).

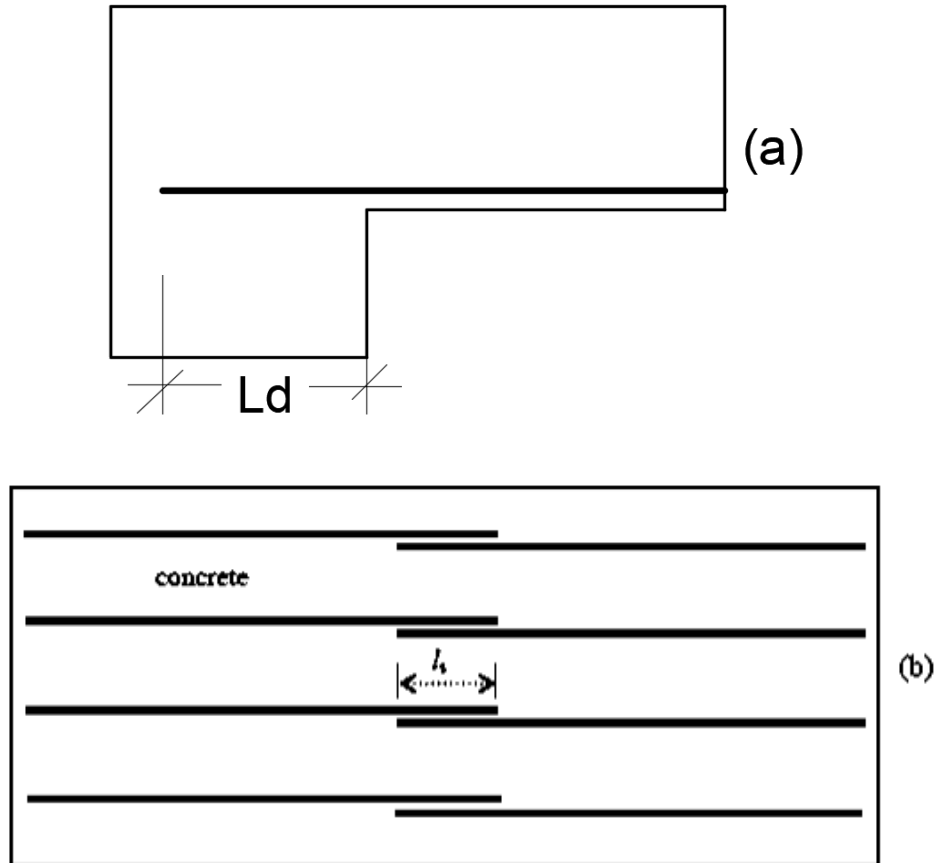


Figure 2.0.1 Typical cases in hand (a)anchorage (b) laps

The required anchorage of a bar in the critical section is commonly referred to as the development length in the design rules and specifications. In Eurocode 2, the tension bar development length is expressed as  $l_{bd}$ , while the corresponding tension bar lap splice is called  $l_o$ . The development length specified for a tensile reinforcement bar should ensure that the member maintains the fundamental requirement of ductility and robustness with the increasing deformation. While the concrete alone can carry the large proportion of the flexural compressive forces, the tensile forces in a flexural member of the RC need to be mostly carried by the reinforcement. If a reinforcing bar is insufficiently anchored, it may result in insufficient

bond stresses to transfer the tensile forces to the bar which, which may result in brittle bond failure by splitting the concrete cover that is often associated with the concrete pull - out bar. However, local bond loss along a partial bar length usually does not result in sudden bond failure if a sufficient length of reinforcement is anchored on either side of the local bond failure region. To ensure strength, ductility and robustness in the performance of the RC structure, the design rules and specifications for anchoring tensile bars (whether a straight development length or a lapped splice length or anchorage involving a hooked cogged bar) are formulated in design codes.

## 2.2 Mechanism of bond transfer between reinforcement and concrete

Many reinforced concrete textbooks explain the fundamental mechanism of bond transfer. (e.g., Ferguson, 1958; Park and Paulay, 1975; Wight and Macgregor, 2012; Fanella, 2011; fib bulletin 10). The bond structural mechanics between concrete and deformed reinforcement bar consists of three basic components:

- i) Chemical adhesion
- ii) Friction
- iii) Mechanical interlocking of concrete against the bar deformations (the lugs around the bar perimeter)

A deformed bar embedded in concrete develops the primary bond through adhesion and a small amount of friction between the concrete and the bar. However, the resistance to adhesion and friction is quickly lost, leaving the stresses to be transferred to the concrete mainly by bearing the bar deformations as shown in Figure 2.2(a).

The pressure (or bearing stress) on the concrete necessarily has a radial (or transverse) longitudinal component as shown in Figure 2.2(c). Like the water pressure in a pipe, the latter causes circumferential tensile stresses. (Figure 2.2d).

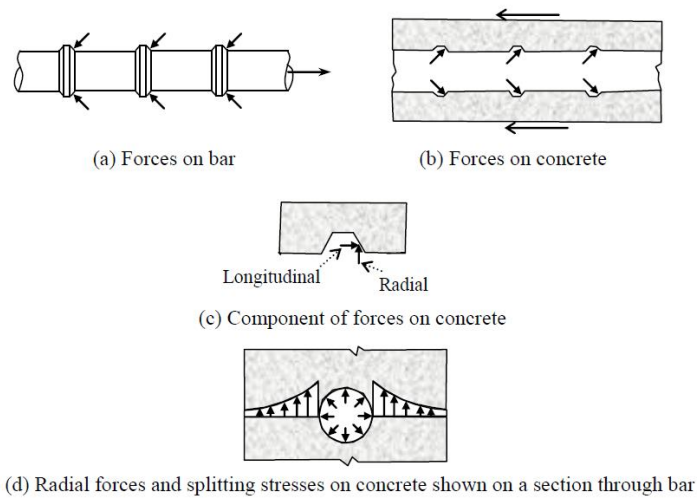


Figure 2.2 Mechanism of bond transfer in reinforced concrete (Wight and Mecgregor 2012)

Since many tests on the pull - out test specimens have been performed, the mechanism on which bar to concrete bond develops is well known for specimens of short anchorage (pull - out). Researchers generally agree that four different stages may characterize the bond between

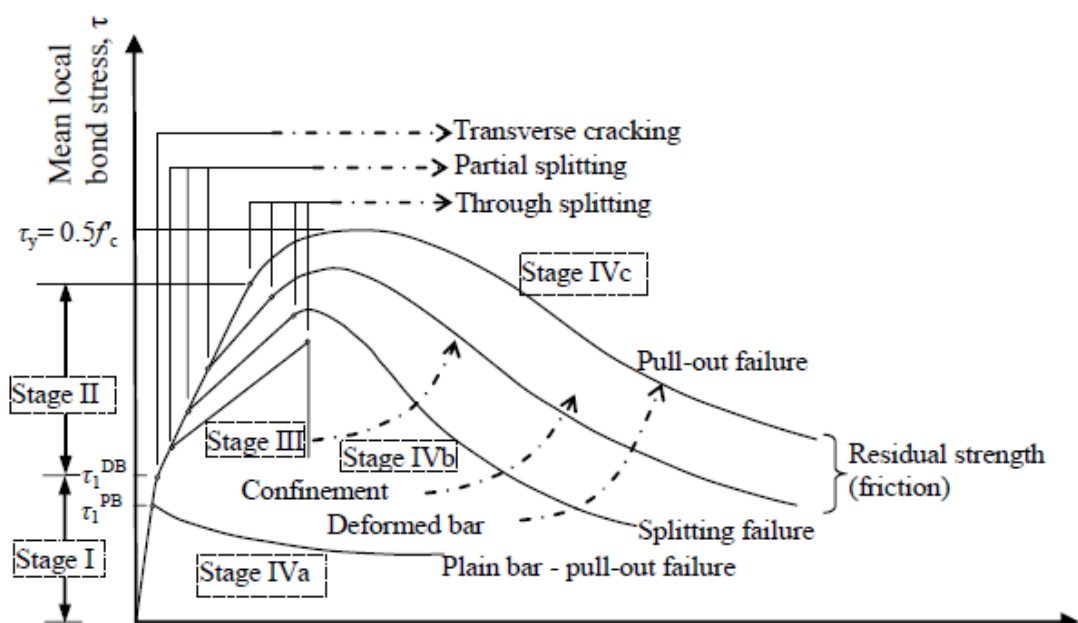


Figure 2.3 Stages of bond resistance in typical bond stress-slip law  $s$

a reinforcing bar and concrete in a pull - out test, and these four stages are represented by four different regions in the mean local bond ( $\tau$ ) versus mean local slip ( $s$ ) relationship proposed by the fib (International Federation for Structural Concrete) and shown in Figure 2.3 (*fib Bulletin 10-2000*).

Stage I (uncracked concrete): For low local bond stress values, this first stage of the bar - to - concrete bond occurs. The bond resistance develops mainly through chemical adhesion, and due to the elastic behavior at this stage highly localized stresses develop near lug tips (Figure 2.4a). Almost no bar slip is associated with the bond stresses at this stage. Similarly, chemical adhesion is associated with the physical adhesion (frictional resistance) that develops between the concrete and the surface of microscopically rough steel. Chemical and physical adhesion play a minor role in plain bars and the bond resistance of these two is soon followed by pull - out bond failure resulting in excessive sliding of bars (dry friction, end of Stage IVa). Any transverse pressure positively affects the transfer of force through friction. Concrete shrinkage and progressive wear of the interface along the sliding plane reduce the radial compressive stresses resulting in lower bond strength.

Stage II (first cracking): The bond by physical and chemical adhesion breaks down completely for deformed bars with a slightly higher value of bond stress. The lugs of the deformed bars induce high bearing stress in the concrete ( $p^*$ , Figure 2.4b) and the first transverse microcracks originate at the tips of the lugs which allow the bar to slip. Due to the located transverse cracks, partial splitting occurs. The wedging action of the lugs, however, remains limited and no thorough concrete splitting occurs.

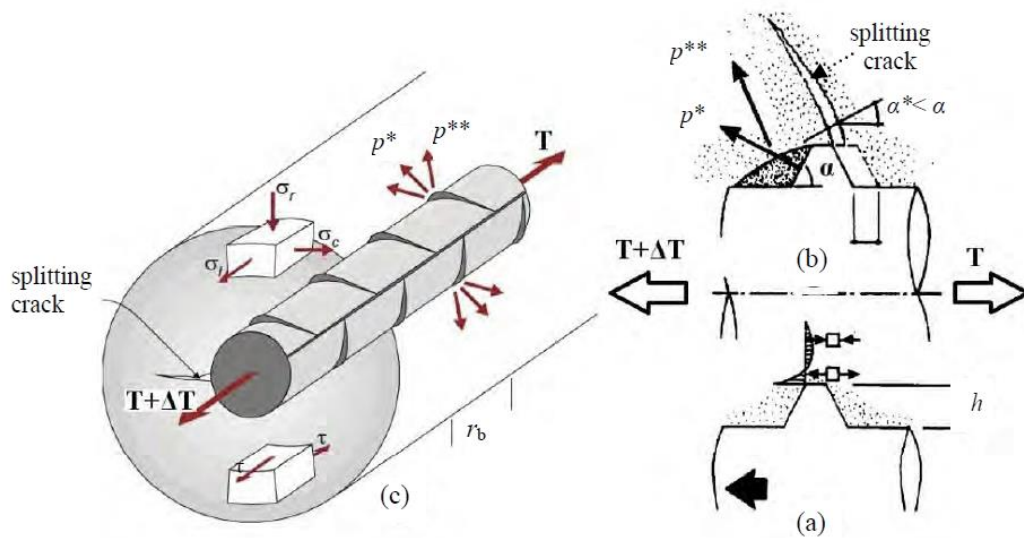


Figure 2.4 Splitting in reinforced concrete: (a) typical stress peaks; (b) bar-concrete slip and wedging action; (c) main parameters

Stage III: The splitting cracks (Figure 2.4c) begin to propagate longitudinally along the bar plane for even higher bond stress values. The angle of inclination ( $\beta$ ) of the bar forces changes due to the concrete crushing in front of the lugs and consequently increases the radial forces / stresses owing to the wedging effect (Gambarova et al., 1996). The surrounding concrete exerts a confining pressure on the bar against the external pressure component ( $p^{**}$ , Figure 2.4b). This phenomenon is conventionally compared with the water pressure that acts against the wall of a thick cylinder that is resisted by the hoop stress in the concrete surrounding it (Tepfers' 1973, 1979, 1982). At this point, the structural components which contribute to the strength and rigidity of the bond are the mechanical interlocking of the lugs, the concrete struts radiating from the bar and the outer concrete ring which is still undamaged. At this stage, the bond resistance is controlled critically by the concrete cover (side or bottom) and the bar spacing (available intact concrete between adjacent bars). The curve to the peak local bond stress may take different paths depending on the transverse containment.

Some unexpected cracking and deformation behavior is usually observed at this stage due to the effects of substantially higher slip values. The global bond failure may be splitting - induced pull - out failure in relatively long anchorages with moderate containment and moderate cover thickness as it does not propagate equally throughout the entire anchorage length through splitting. However, the confining action provided by heavy transverse reinforcement or large concrete cover can be prevented by splitting, and in this case there is exclusive pull - out type bond failure with splitting remaining limited to a cracked core around the bar (Stage IVc).

The bond stress - slip behavior tends to become the type of dry - friction at the end of stage IVb or IVc (Coulomb type), Since the concrete keys are crushed or scraped between the lugs (Figure 2.5) Since the concrete keys are crushed or scraped between the lugs (FIB Bulletin 10-2000). The crushed concrete interface is smoothed as loading continues due to wear and compaction, which increases the splitting stress by further reducing the bond stress. Since global behavior applies to an entire bar, it can result from the superposition of the different stages (Stage I to IV) of bond-slip relationships that may concurrently exist along different sections of the bar. However, as discussed above, the mean local bond stress slip relationships (especially in the range of values of  $T$  and  $s$ ) are derived from short anchorage length specimens test results. The applicability of the  $\tau$ - $s$  relationships outside the range of test data is uncertain since the bond stresses and the splitting stresses are not uniform for longer anchorages, especially considering variable effects caused by crushing and wedging throughout the anchorage.

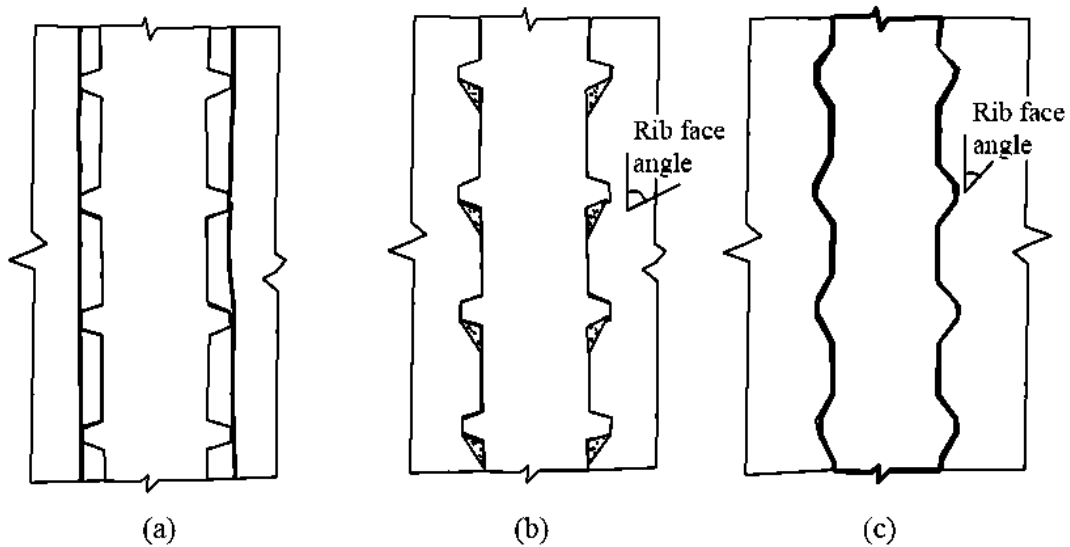


Figure 2.5 Modes of failure: (a) pull-out; (b) splitting-induced pull-out; (c) splitting accompanied by slip

### 2.3 Factors influencing bond stresses and anchorage of reinforcement

The most fundamental factors influencing the anchorage requirements in RC members include concrete tensile strength, distance coverage, spacing of the reinforcing bars and transverse steel reinforcement (Esfahani and Rangan, 2000; Nilson et al., 2004; Wight and Macgregor, 2012). Concrete fracture energy and tensile strength play an important role in bond failure, usually triggered by the spread of a splitting crack in the anchorage region. Cover distance measured either in the bar plane or perpendicular to that plane also affects splitting. If the cover is increased vertically or horizontally, more concrete will be available to resist the tension. Likewise, if the spacing of the bar is increased, more concrete is available per bar to withstand horizontal splitting (Ferguson, 1977). Transverse reinforcement, such as stirrups, improves tensile bar resistance to vertical and horizontal splitting failure. Other factors were also observed to influence the bar anchorage requirements, such as the bar location relative to the member depth ; the presence of transverse pressure within the anchorage zone ; the presence

of any bar coating on the anchored bar, such as epoxy coating ; the inclusion of excess reinforcement over the strength required. Modification factors for these influencing factors, therefore, need to be considered when determining the required development or lapped splice length according to the codes of practice.

#### 2.4 Fundamental theories and factors for anchorage and bond in RC members

Anchorage length or lapped splice length required to develop a particular bar stress,  $\sigma_{st}$ , is here given the symbol  $l_d$  or  $l_s$  (see Figure 2.6). In order to transfer the critical bar force/stresses, a bar must be anchored (or developed) a minimum distance  $l_d$  beyond a critical section according to the fundamental requirement for an anchorage bond. For a typically short anchorage length of a bar, the average bond stress,  $f_b$ , is assumed to be distributed evenly across the bar concrete interface.

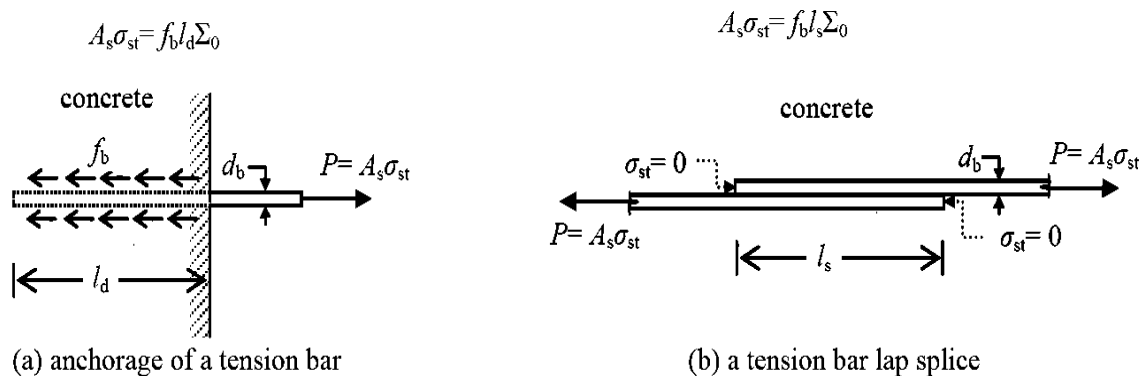


Figure 2.6 Anchorage bond in tension bars

At equilibrium, the bond force is related to the bar force according to the following relationship:

$$f_b \Sigma_0 l_d = A_{st} \sigma_{st} \quad (2.1)$$

Where, as in the bar cross - sectional area,  $\Sigma_0$  is the circumference of the bar and  $\sigma_{st}$  at the critical section is bar stress. The force in bar is calculated by means of the semi - empirical equation described in the following section. From which it is possible to derive equation for bond strength  $f_b$ .

#### 2.4.1 Bar stress - Semi-empirical expression

In a good casting position, it is possible to estimate stresses in a lapped or anchored bar using Eq. 2-2. It can not, however, be used directly in design applications, as it is simply a best - fit expression based on mean strength(MC 20).

$$f_{stm} = 54 \left(\frac{f_{cm}}{25}\right)^{0.25} \times \left(\frac{l_b}{\phi}\right)^{0.55} \times \left(\frac{25}{\phi}\right)^{0.2} \times \left[\left(\frac{c_{min}}{\phi}\right)^{0.25} \times \left(\frac{c_{max}}{c_{min}}\right)^{0.1} \times k_m k_{tr}\right] \quad (2.2)$$

where

- i.  $f_{stm}$  is the estimated stress developed in the bar (mean value)
- ii.  $f_{cm}$  is the measured concrete cylinder compressive strength
- iii.  $l_b$  and  $\phi$  are the bond length and diameter of the lapped or anchored bar respectively,
- iv.  $c_{max}$  and  $c_{min}$  are defined in Fig. 3-2
- v.  $K_{tr} = n_l n_g A_{sv} / (l_b \phi n_b)^2$
- vi.  $n_g$  is the number of groups of links within the lap or anchorage length,
- vii.  $n_l$  is the number of legs of a link in each group which cross the potential splitting failure plane
- viii.  $A_{sv}$  the area of each leg of a link, and
- ix.  $n_s$  the number of bars lapped or anchored at the section
- x.  $n_b$  is the number of individual anchored bars or pairs of lapped bars
- xi.  $k_m$  is an 'effectiveness factor' for link confinement, initially taken as 12

The first part of the expression, i.e. the part outside the square brackets, represents bond strength for base reference conditions of confinement, taken as minimum cover equal to the bar diameter and spacing between bars acting in bond equal to two bar diameters, with no

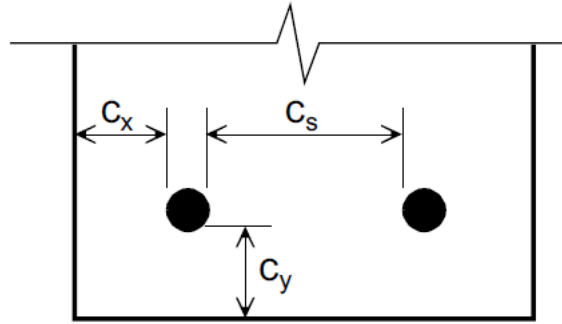
confining reinforcement. A minimum one bar diameter cover is set according to widely accepted detailing practice. The minimum spacing between bars acting in bond is greater than the minimum clear bar spacing stated in MC90, but is consistent with setting a minimum cover of one bar diameter for bond strength as specified in Section 9.1 of MC90. The second ‘confinement’ part of the expression enclosed in square brackets modifies the reference strength for confinements differing from the base level. Defining a good casting position is taken from MC90 and is re - established below

All bars with an inclination of  $45^\circ - 90^\circ$  to the horizontal during concreting and from the bottom or at least 300mm from the top of the concrete layer during concreting.

Limits are set to parameters in Eq. 2-2 as follows:

1.  $15 \text{ MPa} < f_{cm} < 110 \text{ MPa}$ , representing the limits of test data
2.  $K_{tr} \leq 0.05$ , as experimental evidence indicates there to be a threshold value above which no further increase in bond may be obtained, or the rate of increase is markedly lower
3.  $0.5 \leq c_{min}/\phi \leq 3.5$ ,  $c_{max}/c_{min} \leq 5$ , due to lack of experimental data beyond these values Bond length  $l_b \geq 10\phi$

The ratio  $25/\phi$ , representing a diameter-dependent size effect on bond, is limited to a maximum of 2.0 on the basis of evidence in the database. The limitation probably reflects that relative rib area  $f_R$  of small (i.e. 12mm or less) diameter bars is typically lower than that of larger diameters.



$$c_{\min} = \min (c_s/2, c_x, c_y)$$

$$c_{\max} = \max (c_s/2, c_x)$$

Figure 2.7 Definition of concrete covers

#### 2.4.2 Basic bond strength

The basic design bond strength expression is obtained by altering the lead coefficient of 54 in the mean strength expression of Eq. (2.2) to 41 through analysis of the statistical accuracy of the expression. Eq. (2.2) is rearranged to allow bond length  $l_b$  to develop design strength of reinforcement  $f_{yd}=f_{yk}/\gamma_c$  to be determined. Then, the basic bond strength  $f_{bd,0}$  is then obtained by setting the part of Eq. (2.2) in square brackets to a value of 1.0 and dividing bar force  $f_{yd}$ .  $A_s$  by  $\pi \varnothing l_b$ , the nominal bar surface over which  $f_{yd}$  is developed. Likewise, values for cover and confining reinforcement corresponding to minimum detailing requirements are inserted, and indices and coefficients rounded to more convenient values. Bond strength  $f_{bd,0}$  is considered as an average stress on the nominal surface of a straight length of bar over the bond length  $l_b$ . The basic bond strength  $f_{bd,0}$  is:

$$f_{bd,0} = \eta_1 \eta_2 \eta_3 \eta_4 \left( \frac{f_{ck}}{25} \right)^{0.5} / \gamma_{cb} \quad (2.3)$$

where:

- i.  $\eta_1$  is a coefficient taken as 1.75 for ribbed bars (including galvanized and stainless reinforcement), 1.4 for fusion bonded epoxy coated ribbed bars and 0.90 for plain (unribbed) surface bars;

- ii.  $\eta_2$  represents the casting position of the bar during concreting:  $\eta_2 = 1.0$  when good bond conditions are obtained, as for: all bars with an inclination of  $45^\circ - 90^\circ$  to the horizontal during concreting, and all bars with an inclination less than  $45^\circ$  to the horizontal which are up to 250 mm from the bottom or at least 300 mm from the top of the concrete layer during concreting (but see also ‘special circumstances’ section later);
- iii.  $\eta_2 = 0.7$  for all other cases where ribbed bars are used, or
- iv.  $\eta_2 = 0.5$  where plain (unribbed) bars are used;
- v.  $\eta_3$  represents the bar diameter
- vi.  $\eta_3 = 1.0$  for  $\varnothing \leq 25$  mm;
- vii.  $\eta_3 = (25/\varnothing)0.3$  for  $\varnothing > 25$  mm ( $\varnothing$  in mm);
- viii.  $\eta_4$  represents the characteristic strength of steel reinforcement being anchored or lapped;
  - a.  $\eta_4 = 1.0$  for  $f_{yk} = 500$  MPa;
  - b.  $\eta_4 = 1.2$  for  $f_{yk} = 400$  MPa;
  - c.  $\eta_4 = 0.85$  for  $f_{yk} = 600$  MPa;
  - d.  $\eta_4 = 0.75$  for  $f_{yk} = 700$  MPa;
  - e.  $\eta_4 = 0.68$  for  $f_{yk} = 800$  MPa.

Intermediate values may be obtained by interpolation. The partial safety coefficient for bond  $\gamma_{cb}$  is taken as 1.5

### 2.4.3 Design bond strength

The design ultimate bond strength  $f_{bd}$  of ribbed bars may be modified from the basic value where concrete cover, bar spacing or transverse reinforcement differ from their respective minima as stated above, where the bar is subjected to transverse compression or where cracking parallel to the bar axes occurs.

$$f_{bd} = (\alpha_2 + \alpha_3)f_{bd,0} - 2p_{tr} < 2f_{bd,0} - 0.4p_{tr} < \left(\frac{1.5}{\gamma_{cb}}\right) * \sqrt{f_{ck}} \quad (2.4)$$

where:

- i.  $\alpha_2$  and  $\alpha_3$  represent the influence of passive confinement from cover ( $\alpha_2$ ) and from transverse reinforcement ( $\alpha_3$ ). Provided minimum detailing provisions are satisfied,  $\alpha_2$  and  $\alpha_3$  may conservatively be taken as 1.0.
- ii.  $p_{tr}$  is the mean compression stress perpendicular to the potential splitting failure surface at the ultimate limit state; where transverse compression perpendicular to the bar axis acts over a portion of the bond length, bond strength may be increased over that portion.  $p_{tr}$  is negative when transverse stress is compressive.

#### Passive confinement from cover: straight reinforcing bars

$$\text{Ribbed bars: } \alpha_2 = \left(\frac{c_{min}}{\emptyset}\right)^{0.5} * (c_s/2c_{min})^{0.15}$$

$$\text{Epoxy coated bars: } \alpha_2 = \left(\frac{c_{min}}{\emptyset}\right)^{0.7} * (c_s/2c_{min})^{0.15}$$

$$0.5 \leq c_{min}/\emptyset \leq 3, c_s/2c_{min} \leq 5$$

$\alpha_2$  is taken as 1.0 for plain (unribbed) surface bars.

#### Passive confinement from transverse reinforcement

$$\alpha_3 = k_d * \left(K_{tr} - \frac{\alpha_t}{50}\right) \geq 0.0, K_{tr} \leq 0.05$$

- i.  $K_{tr} = n_t A_{st} / (n_b \emptyset s_t)$  is the density of transverse reinforcement, relative to the anchored or lapped bars;
- ii.  $n_t$  is the number of legs of confining reinforcement crossing a potential splitting failure surface at a section;
- iii.  $A_{st}$  is the crosssectional area of one leg of a confining bar [mm<sup>2</sup>];
- iv.  $s_t$  is the longitudinal spacing of confining reinforcement [mm];
- v.  $n_b$  is the number of anchored bars or pairs of lapped bars in the potential splitting failure surface;

vi.  $\emptyset$  is the diameter of the anchored bar or of the smaller of a pair of lapped bars (mm).

#### 2.4.4 Design anchorage length

The stress in the reinforcement to be anchored by bond over the distance  $l_b$  is:

$$\sigma_{sd} = \alpha_1 f_{yd} - \left( \frac{F_h}{A_b} \right) \quad (2.5)$$

where:

- i.  $F_h$  is the force developed by the other measures.  $F_h = 0$  in the case of straight tension bars;
- ii.  $A_b$  is the crosssectional area of the bar considered;
- iii.  $\alpha_1 = A_{s,cal} / A_{s,ef}$  for anchorage or lap-splice zones subject to transverse compression,  $A_{s,cal}$  is the calculated area of reinforcement required by the design and  $A_{s,ef}$  is the area of reinforcement provided;
- iv.  $\alpha_1 = 1.0$  in other circumstances.

The design anchorage length  $l_b$  may be calculated from:

$$L_{sy,tb} = \frac{d_b}{4} \times \frac{\sigma_{st}}{f_b} > l_{b,min} \quad (2.6)$$

#### Minimum anchorage length

Requirement for minimum anchorage length is :

$$l_{b,min} > \max\left\{ \frac{0.3\emptyset f_{yd}}{4f_{bd}}; 10\emptyset; 100mm \right\} \quad (2.7)$$

### 2.5 Eurocode 2

The basic anchorage length,  $L_{sy-tb}$ , for anchoring the force in a straight bar ( $\sigma_{st}A_s$ ) is equal to the perimeter of the bar times the average uniform bond stress  $f_b$  and is given by

$$L_{sy,tb} = \frac{d_b}{4} \times \frac{\sigma_{st}}{f_b} \quad (2.8)$$

where  $\sigma_{st}$  is the design stress required to be developed at the position from where the anchorage is measured from (and equals the yield stress  $f_{sy}$  for the full development length), and the average constant bond stress  $f_b$  is given by

$$f_b = 2.25 \times \eta_1 \times \eta_2 \times f_{ctd} \quad (2.9)$$

where  $\eta_1$  is a coefficient related to the quality of bond and the position of the bar during concreting, with  $\eta_1 = 1.0$  when good conditions are obtained (i.e. bottom bars in beams and slabs, bent-up bars and top bars in thin slabs with less than 250 mm concrete cast below the bar) and  $\eta_1 = 0.7$  for all other cases and for bars in structural elements built with slip forms;  $\eta_2$  is related to bar diameter, with  $\eta_2 = 1.0$  for  $d_b > 32$  mm; and  $\eta_2 = (132 - d_b)/100$  for  $d_b \leq 32$  mm;  $f_{ctd}$  is the design value of the concrete tensile strength and is given by

$$f_{ctd} = \alpha_{ct} \times f_{ctk,0.005} / \gamma_c \quad (2.10)$$

where  $\alpha_{ct}$  is a coefficient taking account of long-term effects and may be taken as  $\alpha_{ct} = 1.0$ ;  $\gamma_c$  is the partial safety factor for concrete ( $\gamma_c = 1.5$ );  $f_{ctk,0.05}$  is the lower characteristic axial tensile strength for concrete given by  $f_{ctk,0.05} = 0.21(f_c)^{2/3}$  for  $f_c \leq 50$  MPa and  $f_{ctk,0.05} = 1.48 \cdot \ln(1 + 0.1(f_c + 8))$  ( $\leq 3.1$  MPa) for  $f_c > 50$  MPa. The design anchorage length is  $s_{y,t}$

$$L_{s_{y,t}} = \alpha_1 \alpha_2 \alpha_3 \alpha_4 \alpha_5 L_{s_{y,tb}} \geq L_{s_{y,t,min}} \quad (2.11)$$

where for a straight anchorage  $\alpha_1 = 1.0$ ;  $\alpha_2 = 1.0 - 0.15(c_d - 3d_b)/d_b$  (but  $0.7 \leq \alpha_2 \leq 1.0$ );  $c_d$  is the smaller of the concrete cover to the deformed bar or half the clear distance to the next parallel bar;  $\alpha_3 = 1.0 - K\lambda$  (but  $0.7 \leq \alpha_3 \leq 1.0$ );  $\lambda = (\Sigma A_{tr} - \Sigma A_{tr,min})/A_s$ ;  $\Sigma A_{tr}$  is the cross-sectional area of

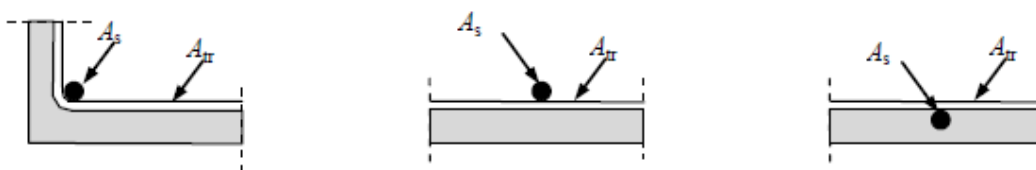


Figure 2.8 Values of K for different bar position

the transverse reinforcement along the development length  $l_d$ ;  $\Sigma A_{tr,min}$  is the cross-sectional area of the minimum transverse reinforcement and may be taken as  $0.25A_s$  for beams and 0 for slabs;  $A_s$  is the cross-sectional area of single anchored bar of diameter  $d_b$ ;  $K$  is given in Figure 2.18(b);  $\alpha_4 = 1.0$  when transverse reinforcement is not welded to the anchored bar (0.7 if it is welded);  $\alpha_5 = 1.0 - 0.04\rho_p$  (but  $0.7 \leq \alpha_5 \leq 1.0$ ); and  $L_{sy-t,min} > \max\{0.3L_{sy-tb}; 10d_b; 100 \text{ mm}\}$ .

The design lapped splice length is

$$L_{sy,t,lap} = \alpha_6 L_{sy,t} \geq L_{s,min} \quad (2.12)$$

where  $\alpha_6 = (\rho_1/25)^{0.5}$ , but not exceeding 1.5 nor less than 1.0;  $\rho_1$  is the percentage of reinforcement lapped within  $0.65l_s$  on either side of the centre of the lapped splice length considered. For  $\rho_1 < 25\%$ ,  $\alpha_6 = 1.0$ ; for  $\rho_1 = 50\%$ ,  $\alpha_6 = 1.4$ ; and for  $\rho_1 > 50\%$ ,  $\alpha_6 = 1.5$ ; and  $L_{s,min} > \max\{0.3\alpha_6 L_{sy-t}; 15d_b; 200 \text{ mm}\}$ .

## 2.6 Effect of Elevated Temperature on Concrete Properties

### 2.6.1 Concrete Compressive Strength

The temperature increase leads to a reduction in concrete strength. This decrease can be explained by different reasons, such as micro and macro cracks on the concrete, the expansion of the aggregate volume and the deterioration of the (C - S - H) gel. In most concrete structures, when the concrete is exposed to high temperatures, the post-cooling strength remains approximately 75% to 25% of the original compressive strength, respectively. [Concrete Society (1990), Phan, L.T. (1996)]. The researcher also noted that the aggregates belonging to the group with a lower thermal expansion than siliceous aggregates such as granite, basalt, calcareous and sea gravel have almost the same compressive strength reduction. The author called the main group the group of concretes made of such aggregates (granite, basalt, calcareous and sea gravel). It was observed that the aggregate concrete of the main group showed higher residual compressive strength values than the silica aggregate concrete. Abrams

(1971) also confirmed that concrete made of silica aggregate above 430 ° C had lost more than concrete made of calcareous or lightweight aggregates, but the difference disappeared when the temperature reached 800 ° C. Xiao et al. (2004) reviewed past research on concrete behavior both under and after exposure to high temperatures. The results showed that the concrete compressive strength fell slightly first under high temperatures of up to 400 ° C and then increased slightly, which could be considered constant. The compressive strength dropped rapidly above 400 ° C. Approximately 80 percent of the original unheated compressive strength was lost at 800 ° C. The behavior of normal strength (27.6 MPa) at high temperatures was investigated by Castillo (1987). All specimens had a heating rate between 7 and 8 ° C / min. The results showed that the peak strain did not differ significantly between 100 and 200 ° C for both concrete strengths. The peak strain increased slightly for temperatures ranging from 300 ° C to 400 ° C. At 800 ° C, the peak strain at ambient temperature was three to four times the peak strain as shown in Figure (2.9).

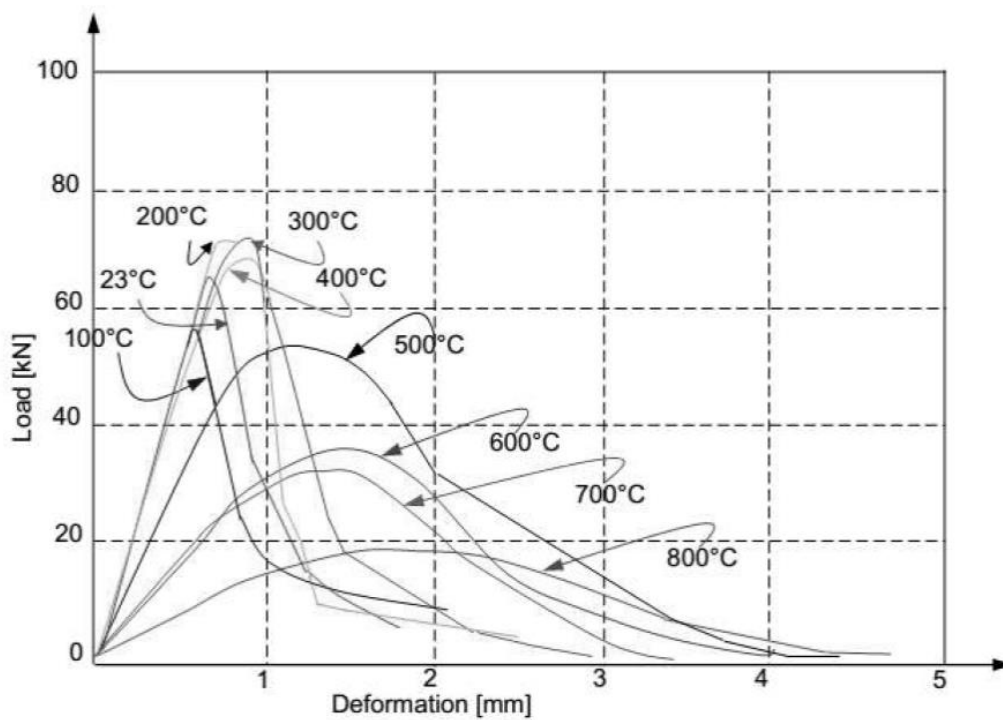


Figure 2.9 Compressive Load Behavior of normal strength concrete at elevated temperature

### 2.6.2 Concrete Tensile strength

The concrete tensile strength is more affected by elevated temperature than the compressive strength. Harada et al. (1972) found that the reduction in compressive strength is lower than that in tensile strength for the same elevated temperature. Thelandersson (1972) studied the effect of elevated temperatures on the concrete tensile strength. It was observed that the tensile strength decreases significantly with increasing temperature in the range of 300- 600°C. The after cooling tensile strength at 600°C was found to be 20 or 30% from the original tensile strength. It was also concluded that the rate of heating has no remarkable effect on the tensile strength. The researcher also observed that the after cooling tensile strength decreases after air cooling. Therefore, the after cooling strength measured immediately after cooling shouldn't be considered in assessing the after cooling load bearing capacity of fire damaged concrete structures.

### 2.6.3 Bond behavior at Elevated Temperature

Although, bond characteristics between concrete and steel is of importance, fewer studies were conducted to determine the behavior of such connections at high temperatures (N. Pinoteau 2011). In previous studies, the test configurations did not accurately model the heating effect under real condition. Moreover, there was also no study of the effect of elevated temperatures on the epoxy-coated rebar. This is important because epoxy-coated rebars are very different from uncoated rebars when it comes to bonding (Elleithy, 1998). In 2019, Muciaccia and Agnoletti et al. carried out pull out tests using two test methods stabilized temperature ST and constant load CL to describe the bond behavior at elevated temperature.

1. Constant load test (CL): a constant load has been applied to the rebar before temperature increases.

2. Stabilized temperature (ST) testing: temperature along the rebar was stabilized before the load was applied.

In the Constant load test (CL) method, the test specimen is heated to a specified temperature. After the concrete specimen has reached a uniform temperature distribution a load is then applied controlling the rate of increase in either stress or strain until failure occurs. The bond behavior was investigated for pre-cast and post-installed rebars. All specimens had a cylindrical shape with height of 200 mm ( $h \approx l_v + 80$  mm) and diameter of 150 mm with concrete class C20/25. The embedding depth of the rebar is 10 times the diameter of the rebar. Two temperature measuring points (Type K thermocouples) were placed from the borehole bottom at 1d (12 mm) and below the concrete surface at 1d (12 mm). The specimen used is presented in Figure (2.10).

The significant decrease in bond capacity detected at high temperatures requires that longer embedded depths be re-designed to meet fire safety standards. Furthermore, a significant thermal variation can be attributed to the effect of water vaporization that is not uniform along

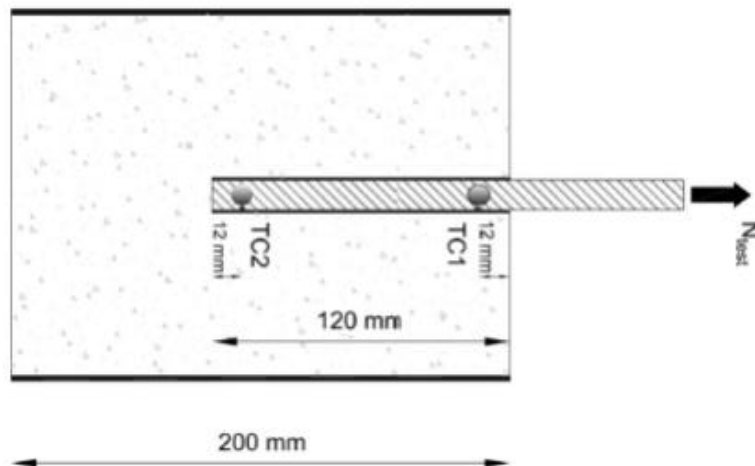


*Figure 2.10 Details of specimen*

the bonded length when testing at constant load. This may result in uneven temperature distribution along the bar, which is a function of the boundary test conditions (N. Pinoteau, 2011).

While stabilized temperature test procedure (ST): after installing the specimen in the oven, the difference lies in the heating and loading sequences. This method has a more uniform and reproducible temperature distribution and to exclude the effects of creep induced by applying a constant load, the possibility of achieving uniform temperature distribution along the rebar before applying the load. However, given a temperature dependent bond strength from experiments ( $\tau_m$ ) it is possible to define a reduction factor  $\chi(T)$  of the (uniform) bond  $\tau_m$  as a function of temperature as

$$\chi(T) = \frac{\tau_m(T)}{\tau_m(20C)} \quad (2.13)$$

the normalized results for constant load method (CL) pullout test are shown in Figure 2.11, where C,S,E are abbreviated for center, side, and edge bar position. This factor can be of key importance as it can be used to reduce design bond strength  $f_{bd(20^\circ C)}$ .

<i>Temperature</i>	<b>30</b>	<b>60.2</b>	<b>71.2</b>	<b>100</b>	<b>200</b>	<b>300</b>	<b>432.4</b>	<b>465.3</b>
$\chi$ center-pc	0.99	0.68	0.64	0.56	0.47	0.44	0.42	0.42
center-pI	1.00	0.83438	0.75194	0.5781				
side-pc	1.00	0.83	0.80	0.74	0.64	0.59498	0.56093	0.5547

In practical fire scenario, structural elements are under load prior to a fire situation. This is perfectly depicted in constant load (CL) test method, where specimen is under load before heating phase. While in standard temperature (ST) test method, element is heated up to a certain degree and then subjected to loading. Therefore, results from CL method are used in this thesis work.

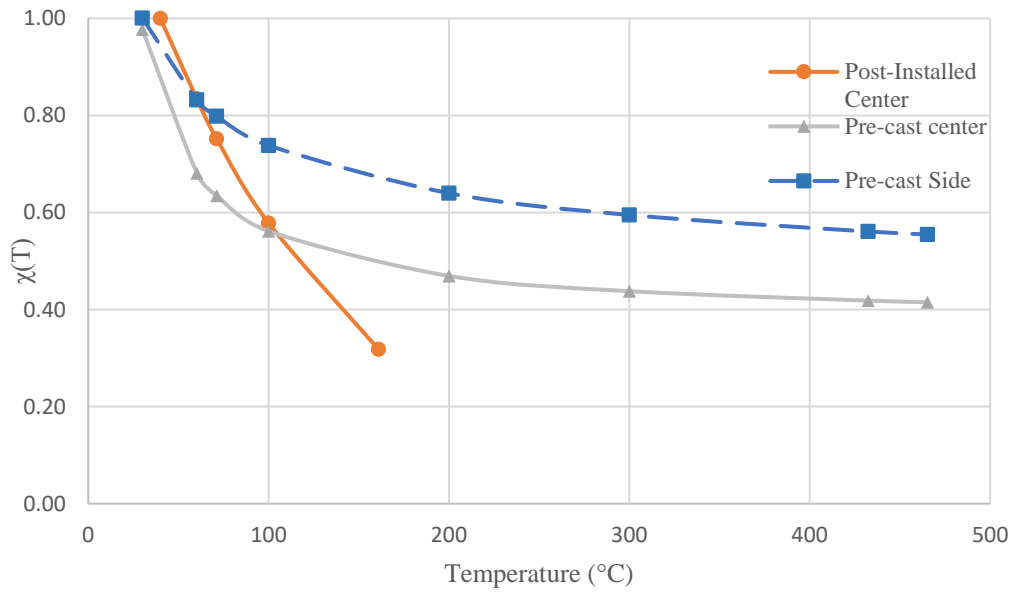


Figure 2.11 Reduction Curves for pre-cast and post-Installed rebars (Muciaccia )

# Chapter 3

## Analysis Methodology

### 3.1 Heat transfer analysis

In order to find the temperature contours for a certain geometric connection configuration as shown in Figure 3.1 at different times of fire exposure, heat transfer analysis can be performed either through finite element analysis or finite difference method. Information on temperature distribution then can be used to find reduction factor for a certain segment.

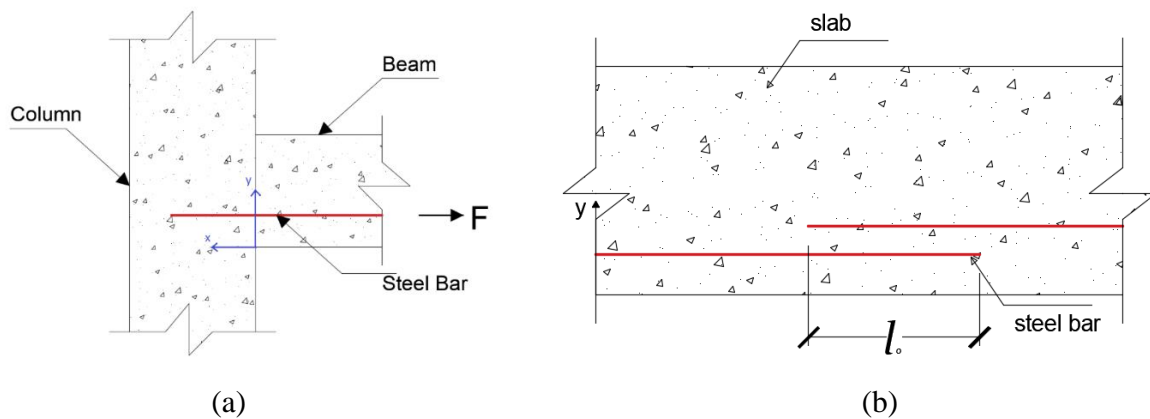


Figure 3.1 Investigated cases: (a) anchorage at beam-column node; (b) lap splice

It is important to know the thermal properties of concrete, irrespective of the method of analysis chosen, by conducting appropriate tests or using design codes.

#### 3.1.1 Modelling parameters

Concrete thermal properties such as thermal conductivity ( $\lambda(\theta)$ ), specific heat  $C_p(\theta)$  and material density can be directly found in design guides such as Eurocode 2 part 1-2:

$$\rho(\theta(x, t)) \cdot C_p(\theta(x, t)) \cdot \frac{\partial(\theta(x, t))}{\partial t} = \lambda(\theta(x, t)) \cdot \frac{\partial^2(\theta(x, t))}{\partial x^2} \quad (3.1)$$

$$q_{\text{conv}} = h(\theta_{\text{ext}}(x, t) - \theta_{\text{surf}}(x, t)) \quad (3.2)$$

$$q_{\text{rad}} = \sigma \cdot \varepsilon (\theta_{\text{ext}}^4(x, t) - \theta_{\text{surf}}^4(x, t)) \quad (3.3)$$

Where

$\rho$  is the material density [kg/m<sup>3</sup>].

$C_p$  is the material specific heat [JK<sup>-1</sup>kg<sup>-1</sup>]

$\lambda$  is material thermal conductivity [Wm<sup>-1</sup>K<sup>-1</sup>]

$\Theta(x,t)$  is the temperature of an element at position  $x$  and time  $t$  [K]

$q_{\text{conv}}$  is convective heat flux [W m<sup>-1</sup>]

$q_{\text{rad}}$  is radiative heat flux [W m<sup>-2</sup>]

$h$  is the heat transfer coefficient [W m<sup>-2</sup> K<sup>-1</sup>]

$\sigma$  is Stefan-Boltzmann constant [Wm<sup>-2</sup>K<sup>-4</sup>]

$\varepsilon$  is emissivity of the material

$\theta_{\text{ext}}$  is the gas temperature [K]

$\theta_{\text{surf}}$  is the temperature at the surface of the material [K]

Following Eurocode 2 suggestions [6],  $\varepsilon$  for exposed and unexposed side is taken as 0.7, while

$h$  for exposed side is 25 W/m<sup>2</sup>K and for unexposed side it is 4 W/m<sup>2</sup>K.

Specific Heat	Temp.	Conductivity	Temp.
900	20	1.95	20
900	99.99	1.772	100
1470	100	1.55	200
1470	115	1.388	300
1000	200	1.232	400
1100	500	1.042	500
1100	1000	0.992	600
-	-	0.908	700
-	-	0.848	800
-	-	0.812	900

*Table 1. Specific Heat and Conductivity*

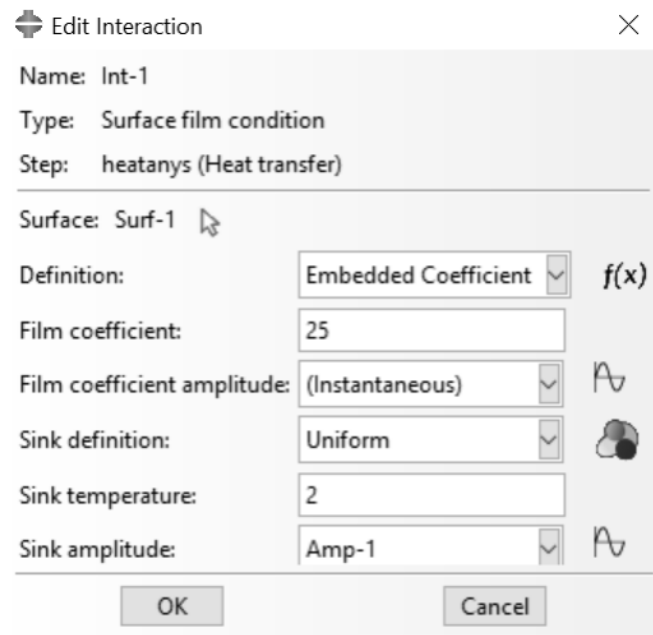


Figure 3.3 Conductive Boundary condition for exposed surface

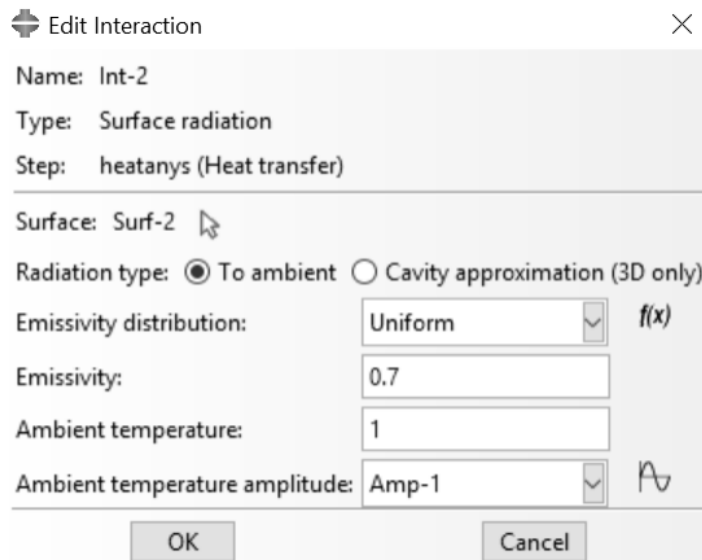


Table 3.2 Surface radiation for exposed side

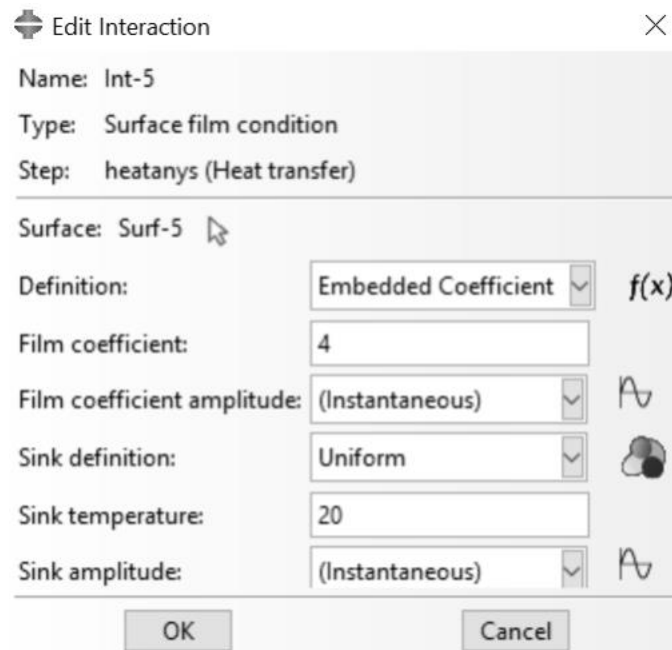


Table 3.3 Boundary condition for unheated surface

### 3.1.2 Fire Modelling

Evaluation of temperature during fire event is usually based on the standard ISO 834 time-temperature curve. Recent research has shown that the actual building elements exposed to real building fires is substantially lower than the so called standard fire scenario. However, for simplicity, thermal actions were modelled using conventional temperature/time relationship (ISO834-1):

$$T_g = T_o + 345 \log_{10}(8t + 1) \quad (3.4)$$

Where

$T_g$  is gas temperature

$T_o$  is initial temperature (20°C)

t is time in minutes.

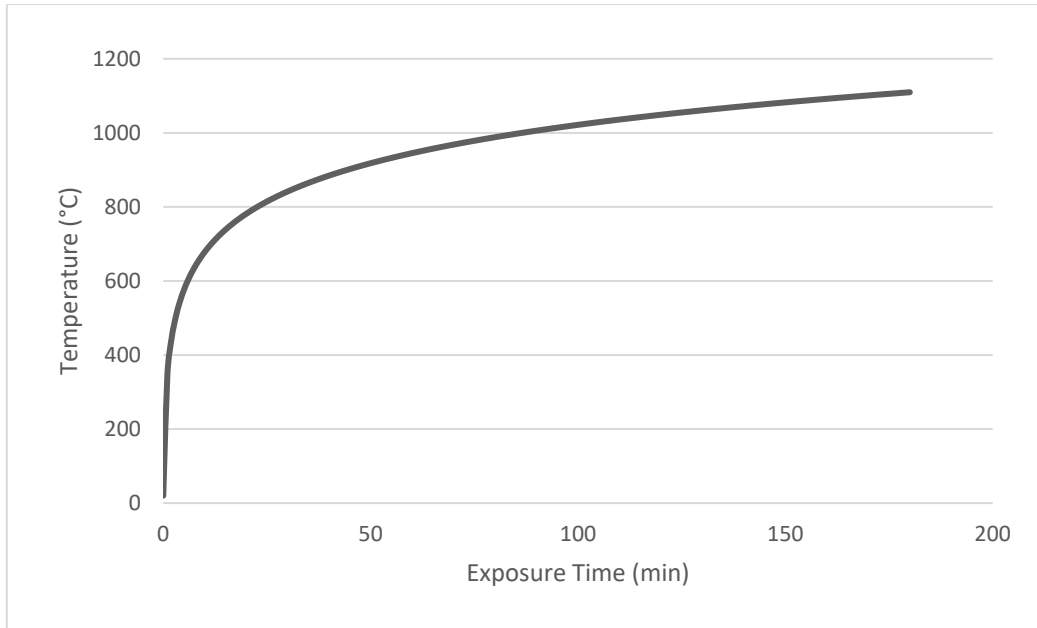


Figure 3.6 Standard fire curve ISO 834-1

**Edit Amplitude** ✕

Name: Amp-1

Type: Tabular

---

Time span: Step time v

Smoothing:  Use solver default  
 Specify:  

Amplitude Data Baseline Correction

	Time/Frequency	Amplitude	^
1	0	20	
2	60	349.2136658	
3	120	444.5048779	
4	180	502.289303	
5	240	543.8873093	
6	300	575.4104205	v

OK
Cancel

Figure 3.7 Fire curve input as amplitude

### 3.1.3 Numerical Modelling

The analysis is carried out in Abaqus 2018 and the reference structure is chosen to be a concrete beam-column connection with a thickness of 0.1m and width of 0.3 m each side. Each edge is divided in 10 finite elements, and a finer meshing of 0.03 seed at beam-column connection, with an element type DC3D20 (3D linear quadratic). Figure 3.8 demonstrate sample meshed element, and sample result for temperature profile at exposure time R120 is shown in Figure 3.9. In addition, environmental temperature interactions take into account the heated (bottom) surface and the unheated (top) surface. The convective heat coefficient for the heated surface is defined by 25 W/m<sup>2</sup>K and 0.7 emissivity. For convective and radiative heat transfer, the unheated surface interactions are 4 W/m<sup>2</sup>K and 0.7 respectively.

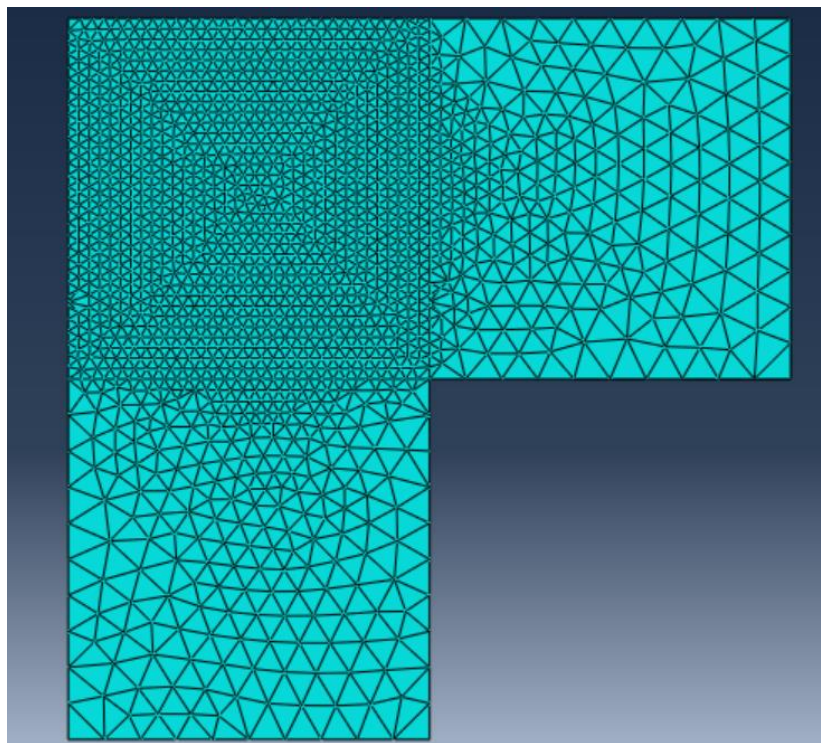


*Figure 3.8 Sample meshed element*

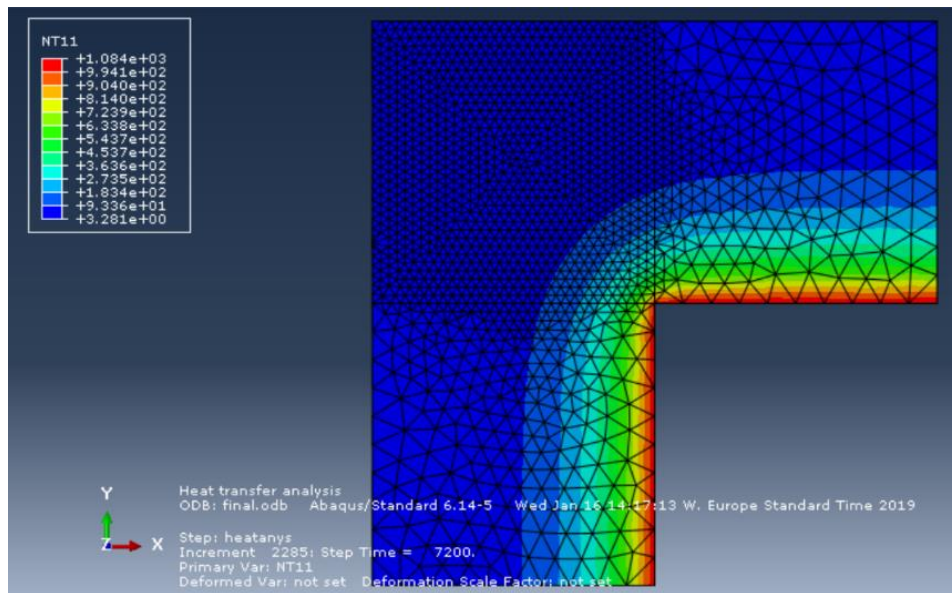


*Figure 3.9 Temperature profile for time 120 minute*

### 3.1.4 General Observations

At beam-column connection, temperature values for different time exposure such as R30, R60, R90 and R120 were extracted from analysis result as arrays and matrices. where temperature ( $T$ ) was varying both on embedded length  $x$  (mm) and edge distance  $y$  (mm), Figure 3.10 shows temperature distribution  $T(x,y)$  at the connection for exposure time R120.

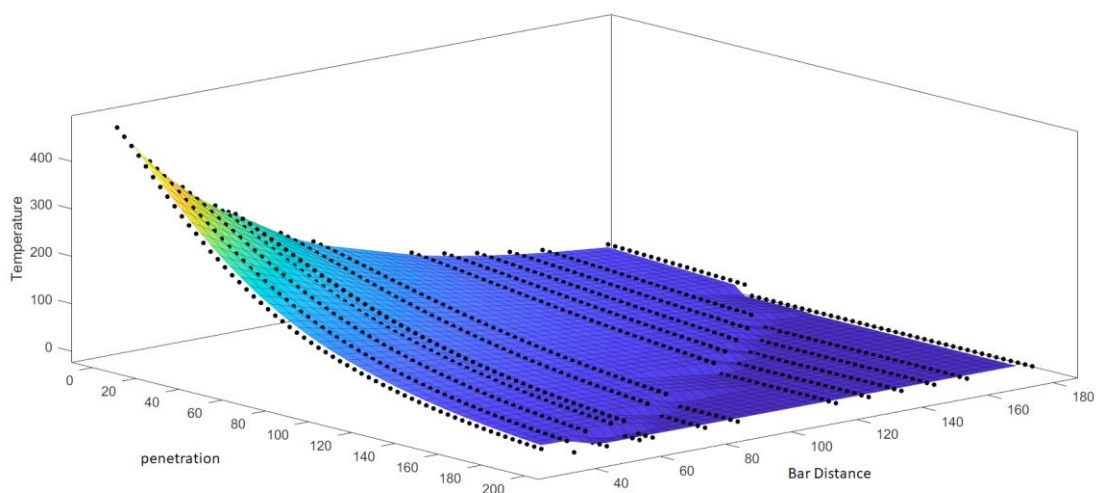


*Figure 3.10 Temperature distribution at time R120 for different edge distances at beam-column connection*

Figure 3.12 represents a sample temperature gradient for different exposure times along the embedded length at the edge distance of 30 mm. As expected, going farther from the exposed surface temperature decreases in a non-linear trend. Note that temperature values should only be seen only along abscissa starting from the exposed surface till the point where ambient temperature is achieved; as beyond this, fire does not affect the bond strength. This value depends on the considered exposure time, specifically it increases for increasing exposure time as represented in the figure.

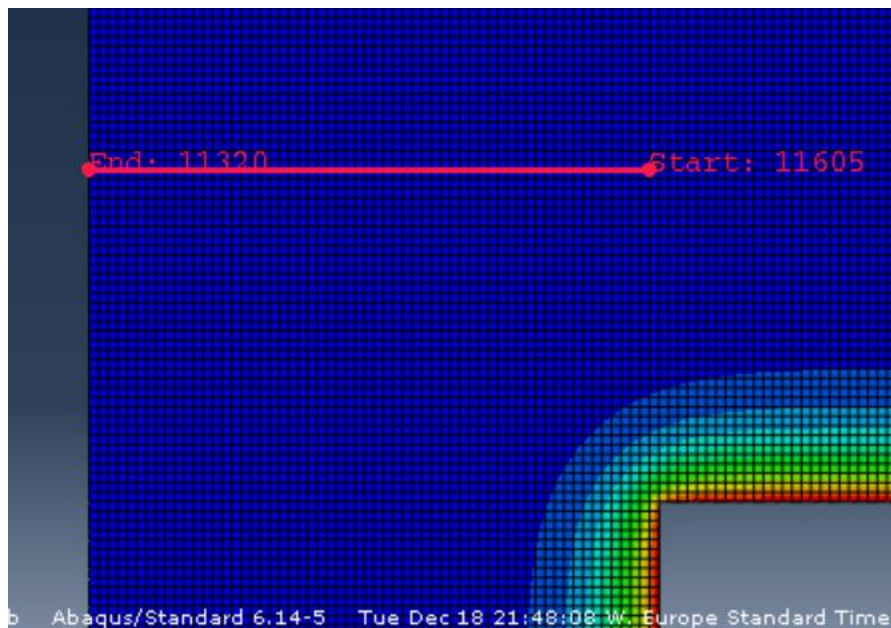


*Figure 3.11 Temperature Path selection*

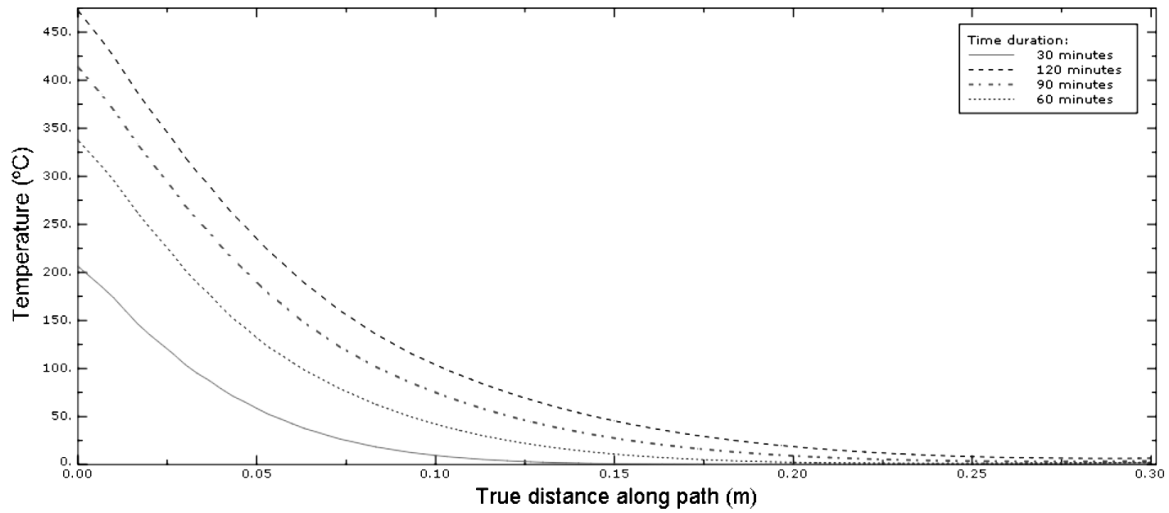


Figure 3.12 Temperature gradient at 30 mm edge distance

Temperature curves i.e.  $T(x)$  for different values of edge distance are shown in Figure 3.13 at exposure time of 120 minutes. Here the distances are taken at multiples of 30 or twice of bar diameter. It can be noted that as moving along the edge distance (y-axis), maximum temperature drops significantly.

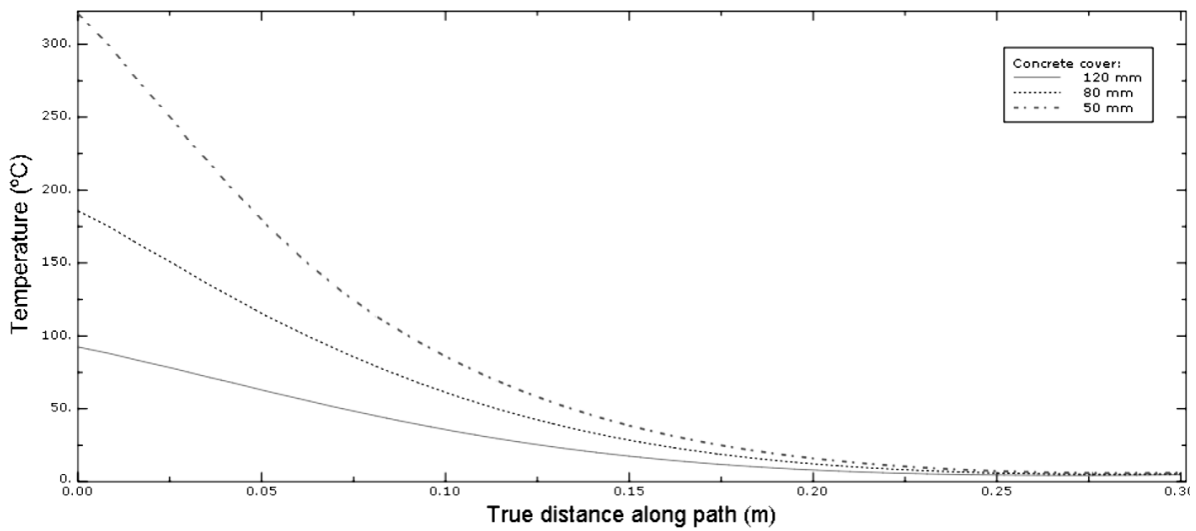
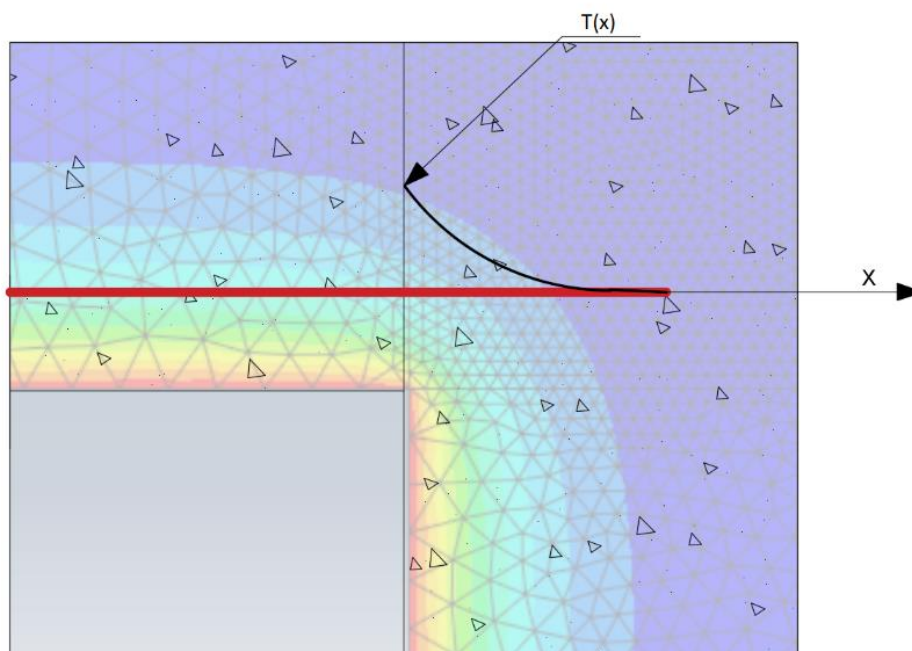


Figure 3.13 Temperature gradient for time 120 minute

## 3.2 Proposed scheme for incremented embedded length

### 3.2.1 Anchorage at beam-column connection

Now that temperature profiles are created at different exposure times, length increment can be calculated using reduction curves for various cases such as pre-cast or post-installed and centre, side or edge bar position in the procedure described below. In addition, a demonstration for temperature distribution along the bar is shown in Figure 3.14.



*Figure 3.14 Anchorage at beam-column node, example of temperature distribution along the bar*

Subsequently, for a given value of edge distance ( $y$ ), which here can be maximum of multiple of 30 or twice the bar diameter, temperature dependent bond strength is obtained along the bond interface by multiplying  $f_{bd,20^{\circ}C}$  by the reduction factor  $\chi(T(x))$  employing the following relation:

$$f_{bd,T(x)} = \chi(T(x)) \times f_{bd,20^{\circ}C} \frac{y_m}{y_{m,fi}} \quad (3.5)$$

Where

$\gamma_{M,fi}$  is the material partial safety factor under a fire case and is taken as equal to 1 [6]

$f_{bd,T(x)}$  = is reduced bond strength due to temperature distribution  $T(x)$  along the embedded length

$\chi$  = is a case specific, empirical value of strength reduction factor

Values of temperature  $T(x)$  are taken from temperature profiles obtained in previous step that can vary along the embedded length. Extrapolation is not possible for temperature values higher than those reported in reduction curves, so  $\chi(T(x))$  is taken as zero at higher temperatures.

The required increment in anchorage length  $\Delta L_d$  to transfer a force  $F_{applied}$  in a corner at of a beam-column node is then calculated as follows:

$$\Delta L_d = \frac{A_1 + A_2}{f_{bd(20^\circ C)}} \quad (3.6)$$
$$F_{applied} = \pi \times \emptyset \int_0^{L_d + \Delta L_d} f_{bd,T(x)} dx$$

Where:

$\Delta L_d$  = is an increment in embedded length to sustain applied load [mm]

$A_1, A_2$  = are the areas demonstrating the amount of  $f_{bd20c}$  strength lost during a fire situation.

$F_{applied}$  = is a tensile force sustained by a rebar.

$L_d$  = is an design anchorage length at ambient temperature

$\emptyset$  = is a diameter of rebar.

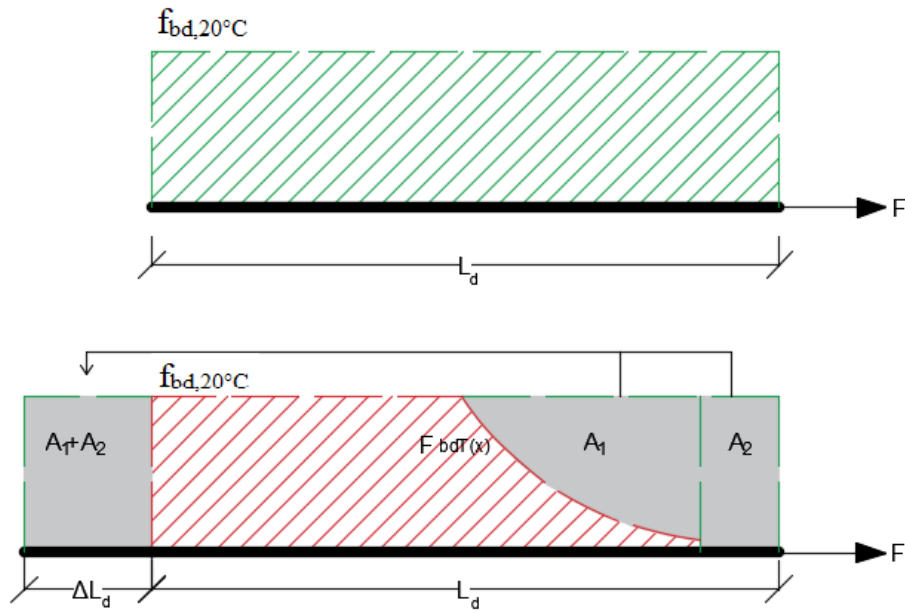


Figure 3.15 Bond strength distribution along the bar

A pictorial depiction of the employed methodology is presented in Figure 3.15 for the ease of understanding. Calculations were performed on MATLAB 2017. Anchorage length that caters the temperature's effect  $L_{d(T)}$  is finally obtained as:

$$L_{d(T)} = L_{d(20°C)} + \Delta L_d \quad (3.7)$$

### 3.2.2 Laps

The level of complexity drops for finding amplification factor for laps. This is due to the fact that in such case temperature does not vary along the lap length, and it only varies as a function of the distance from the exposed surface. Therefore, given a certain value of edge distance,  $f_{bd(T)}$  can be directly used to find the required length increment.

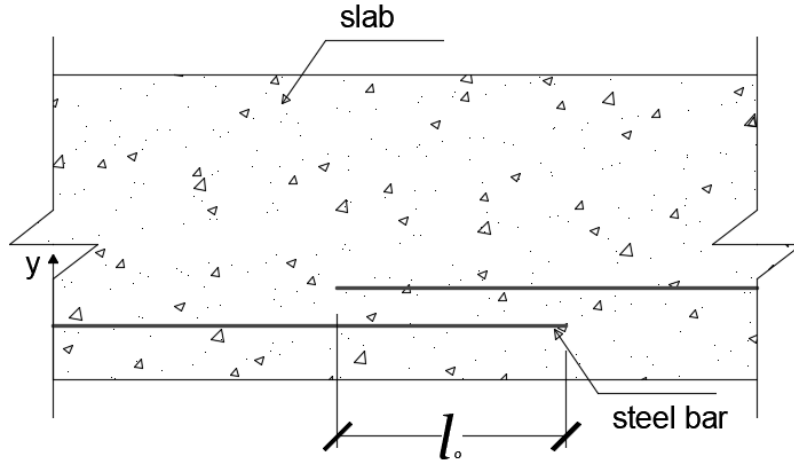


Figure 3.16 Demonstration of laps in a slab

### 3.3 Amplification factor

Provided that the length increment that will accommodate the effects of temperature induced damage, a factor can be proposed for both cases (Anchorage at beam-column connection and Laps) that can be multiplied with basic anchorage length  $L_{d(20^{\circ}\text{C})}$  or basic lap length to get a new embedded length  $L_{d(T)}$ . For anchorage length at beam-column connection node an amplification factor which multiplies the basic anchorage length  $L_{d(20^{\circ}\text{C})}$  to obtain the anchorage length at a given temperature may be defined as follows:

$$\alpha(T) = \frac{L_{d(T)}}{L_{d(20^{\circ}\text{C})}} \quad (3.8)$$

However, it is important to note that  $\alpha$  can vary for different exposure time, bar diameter, edge distance and presence of transversal confinement.

However, amplification factor for laps can be computed simply by using the relation described below and the difference with the previous case is due to constant  $f_{bd(T)}$  across the lapped length:

$$\alpha = \frac{L_{d(T)}}{L_{d(20^{\circ}\text{C})}} = \frac{1}{\chi(T(y))} \quad (3.9)$$

# Chapter 4

## Results

### 4.1 Bond strength $f_{bd(T)}$ distribution

Bond strength  $f_{bd(T)}$  is obtained employing the described scheme using the temperature data obtained numerically. Detailed algorithm for this problem is attached at the end of this thesis document. Results are plotted along the embedded length, for different exposure time, starting from the exposed surface to the point where the bond strength reaches the standard value at ambient temperature  $f_{bd(20^{\circ}\text{C})}$  (Figure 4.1.).

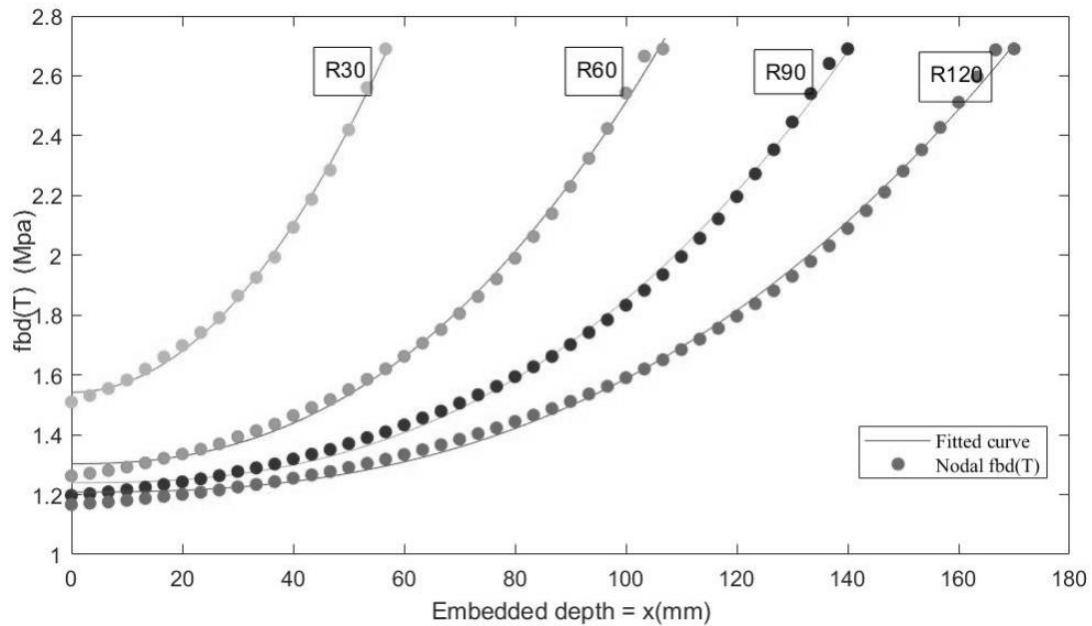


Figure 4.1 Bond strength distribution along the rebar length for pre-cast side

Bond strength distribution for different concrete cover is demonstrated in Figure 4.2, it can be noted that for increasing edge distance from the exposed surface, the magnitude of damaged for a bond strength significantly decreases, which leads to lowering the amplification values for length increment.

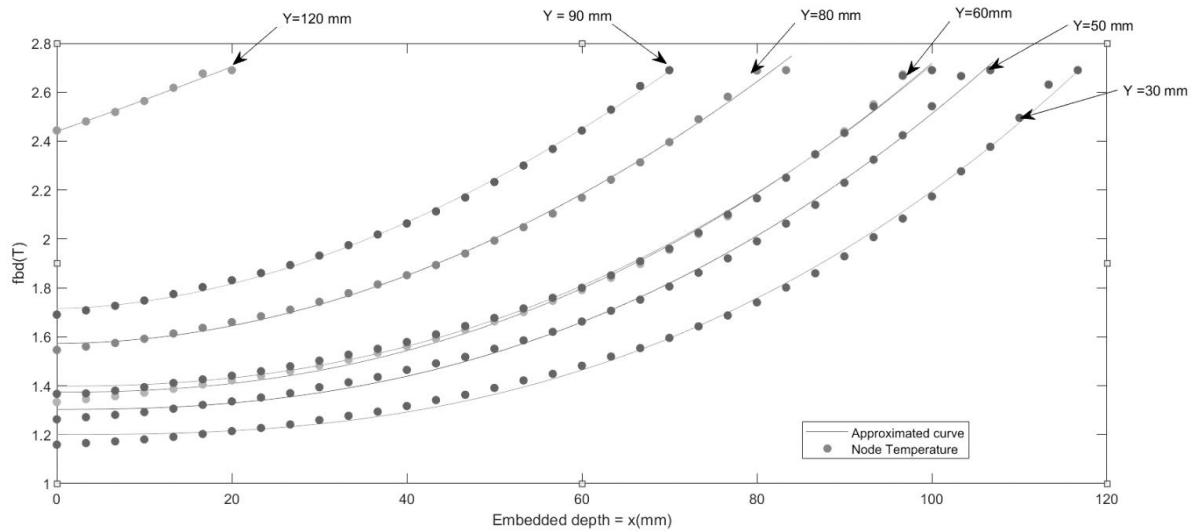


Figure 4.2 Bond strength distribution at different edge distance (Y)

## 4.2 General observations

### 4.2.1 Pre-cast rebars

Amplification factor values for a pre-cast rebar 16mm locate at 80 mm distance from the edge as a function of exposure time is reported in Figure 4.4. The evaluation if carried out considering two different reduction  $\chi(T(x))$ , for a rebar located in the center or at the side, respectively, as reported in Figure 2.11. As it can be noticed, the ‘center’ case is characterized by a higher amplification factor than the ‘side’ case, coherently with the behavior reported in Figure 4.4, due to the presence of transversal reinforcement in the proximity of the bar for the ‘side’ case, which contributes to the load carrying capacity.

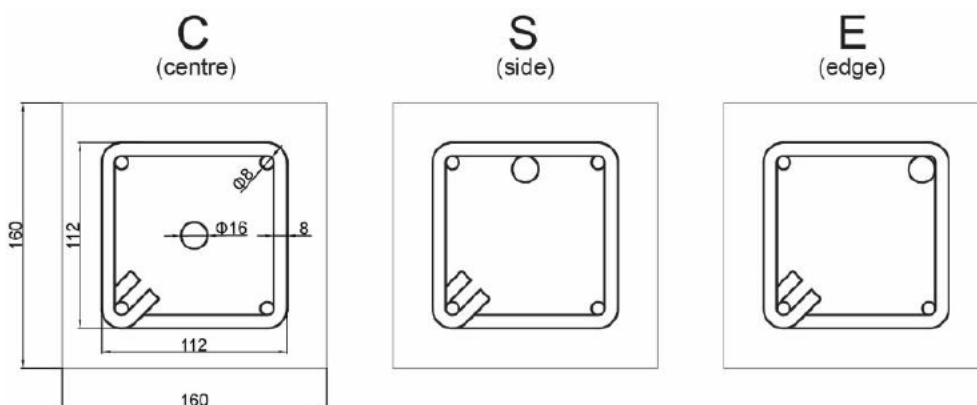


Figure 4.3 Geometry of the transversal section of the specimens

	<b>R30</b>	<b>R 60</b>	<b>R 90</b>	<b>R 120</b>
<i>16</i>	1.00	1.04	1.07	1.09
<i>(mm)</i>	1.00	1.02	1.04	1.06

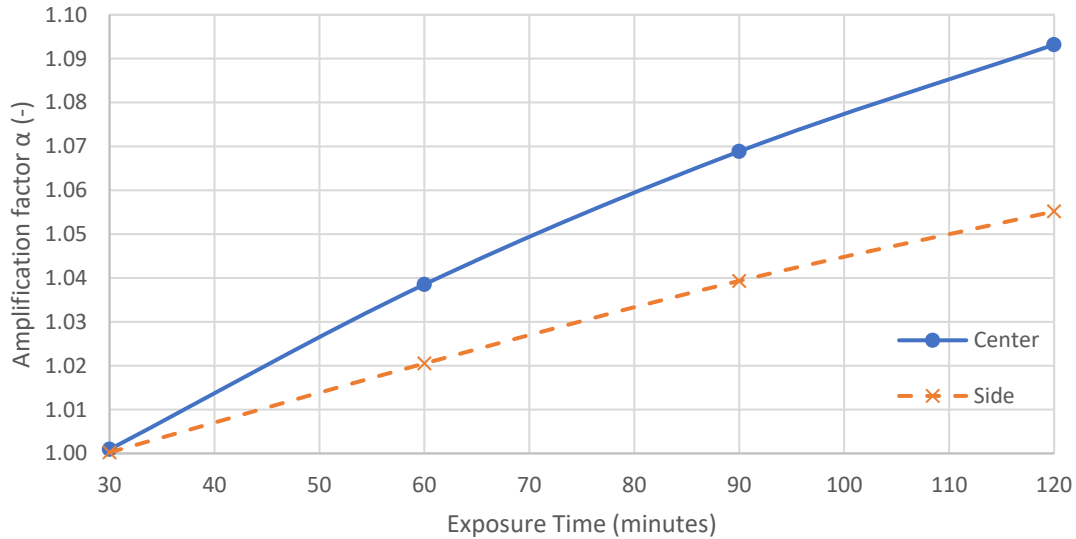


Figure 4.4 Amplification factor pre-cast rebar, as a function of exposure time, rebar diameter  $\phi 16$  and edge distance 80 mm

#### 4.2.2 Post-Installed rebars

The amplification factors  $\alpha$  for pre-cast and post installed bars of diameter 16mm at edge distance of 80 mm are shown in Figure 4.5. For exposure time lower than 110 minutes,  $\alpha$  is significantly lower for the post-installed case. This effect is due to the different shapes of reduction curve for the considered post-installed case which starts decreasing at a relatively higher temperature than for pre-cast rebars. However, for cases where the temperature increases over 100 °C (not represented), the decay for the post-installed case is much more significant and the trend is inverted.

	<b>R30</b>	<b>R 60</b>	<b>R 90</b>	<b>R 120</b>
<i>16</i>	1.00	1.02	1.06	1.10
<i>(mm)</i>	1.00	1.04	1.07	1.09

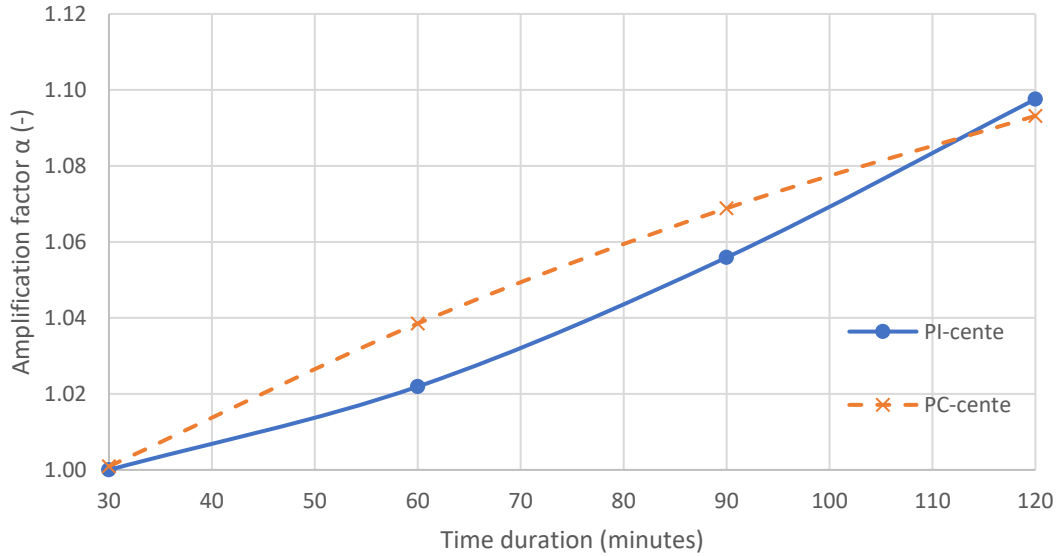


Figure 4.5 Amplification factor for pre-cast and post-installed rebars at edge distance 80 mm

### 4.3 Amplification factor vs Bar diameter

It can be seen in Figure 4.6-4.8 that amplification factor drops significantly as bar diameters increases. This is due to the fact that value of anchorage length increases for larger bar diameters meaning thereby the larger portion of embedded length is in area of bond strength with ambient value  $f_{bd20C}$ . Thus, a little increment can cater the effect of temperature in this case. Moreover, by increasing the edge distance the magnitude of amplification factor drops though the trend remains the same.

Table 4 Amplification factor for pre-cast side at edge distance of 60 mm

<b>Diameter (mm)</b>	<b>R 30</b>	<b>R 60</b>	<b>R 90</b>	<b>R 120</b>
8	1.02	1.07	1.10	1.13
10	1.01	1.05	1.08	1.11
12	1.01	1.04	1.07	1.09
14	1.01	1.04	1.06	1.08
16	1.01	1.03	1.05	1.07
20	1.01	1.03	1.04	1.05
25	1.01	1.02	1.03	1.04
28	1.01	1.02	1.03	1.04
32	1.00	1.02	1.03	1.03

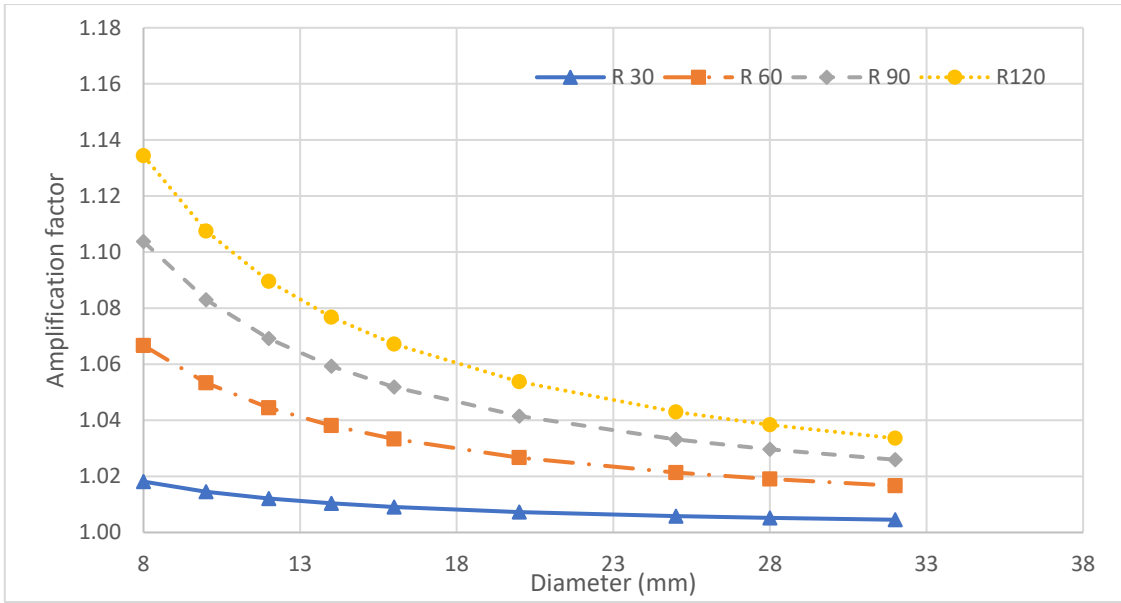


Figure 4.6 Amplification factor for different diameters at 60 mm edge distance

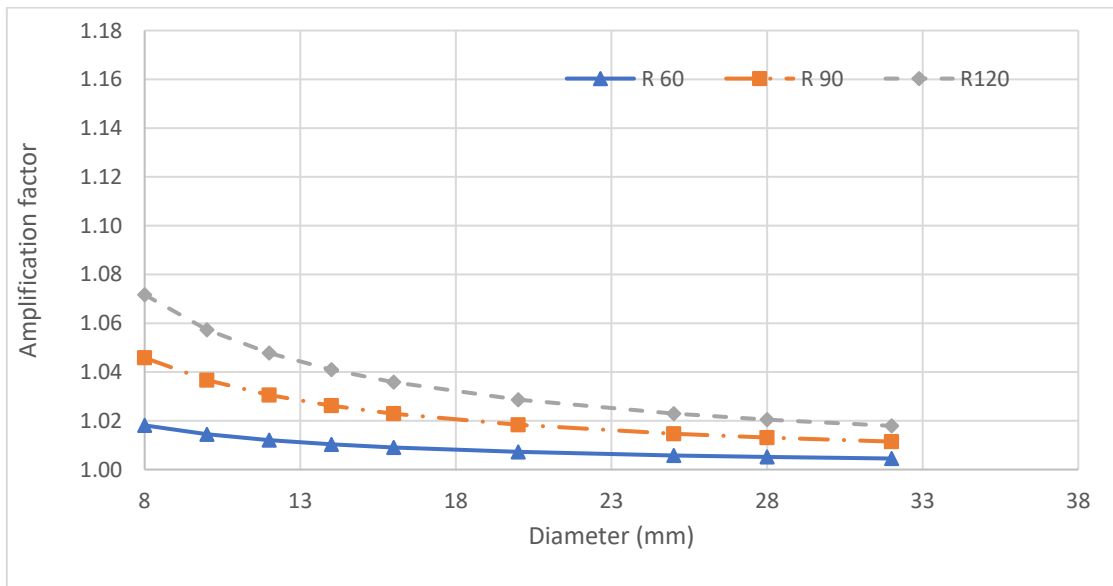


Figure 4.7 Amplification factor for different diameters at 90 mm edge distance

Table 5 Amplification factor for different diameters at 90 mm edge distance

<b>Diameter</b>	<b>R 30</b>	<b>R 60</b>	<b>R 90</b>	<b>R 120</b>
8	1.00	1.02	1.05	1.07
10	1.00	1.01	1.04	1.06
12	1.00	1.01	1.03	1.05
14	1.00	1.01	1.03	1.04
16	1.00	1.01	1.02	1.04

20	1.00	1.01	1.02	1.03
25	1.00	1.01	1.01	1.02
28	1.00	1.01	1.01	1.02
32	1.00	1.00	1.01	1.02

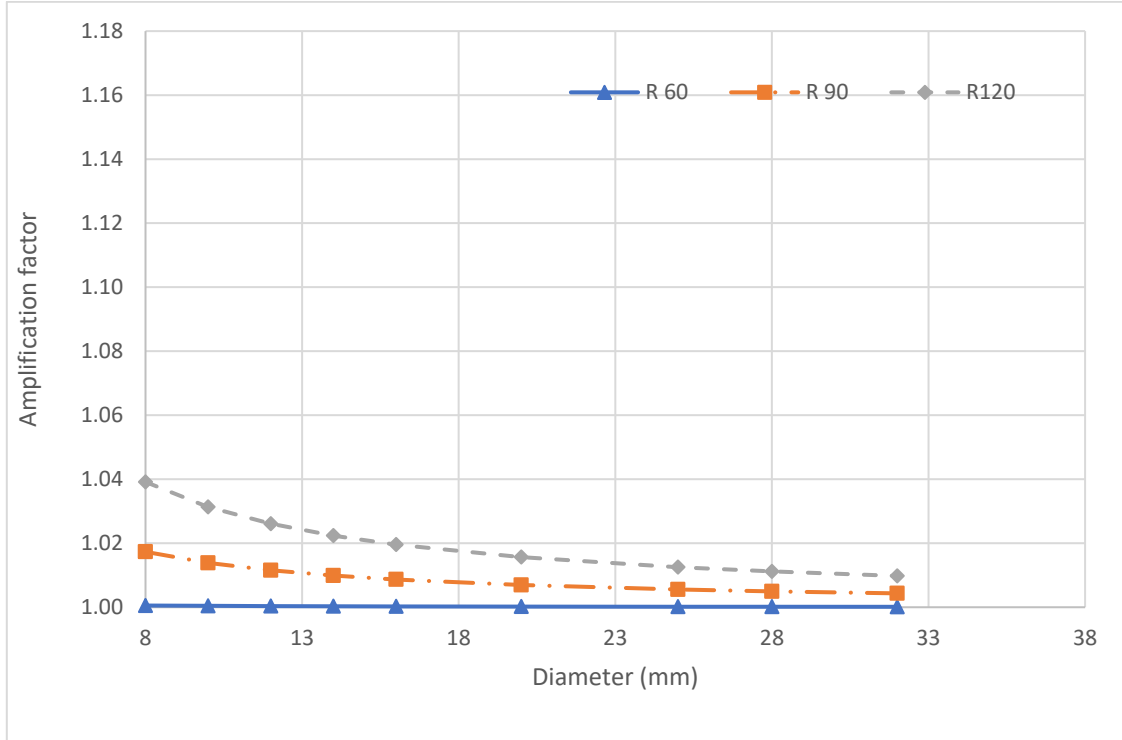


Figure 4.8 Amplification factor for different diameters at 120 mm edge distance

Table 6 Amplification factor for different diameters at 120 mm edge distance

Diameter	R 30	R 60	R 90	R 120
8		1.00	1.02	1.04
10		1.00	1.01	1.03
12		1.00	1.01	1.03
14		1.00	1.01	1.02
16		1.00	1.01	1.02
20		1.00	1.01	1.02
25		1.00	1.01	1.01
28		1.00	1.00	1.01
32		1.00	1.00	1.01

#### 4.4 Amplification factor vs concrete cover

Calculations are performed for amplification factor  $\alpha$  at increasing values of edge distances for bar diameters in the conventional range of 8 – 32 mm and on the basis of the reduction factor for all three cases of pre-cast (Figure 1). In Figures from 4.9 to 4.15, results for a exposure time of 30 to 120 minutes are reported for pre-cast side, edge and center case. It can be observed that, by increasing edge distance,  $\alpha$  is converging to one.

*Table 7 Amplification values for different bar diameters at exposure time R30*

Diameter	concrete Cover (mm)					
	30	40	50	60	64	90
8	1.05	1.04	1.03	1.02	1.02	1.00
10	1.04	1.03	1.02	1.01	1.01	1.00
12	1.04	1.03	1.02	1.01	1.01	1.00
14	1.03	1.02	1.02	1.01	1.01	1.00
16	1.03	1.02	1.02	1.01	1.01	1.00
20		1.02	1.01	1.01	1.01	1.00
25			1.01	1.01	1.00	1.00
28				1.01	1.00	1.00

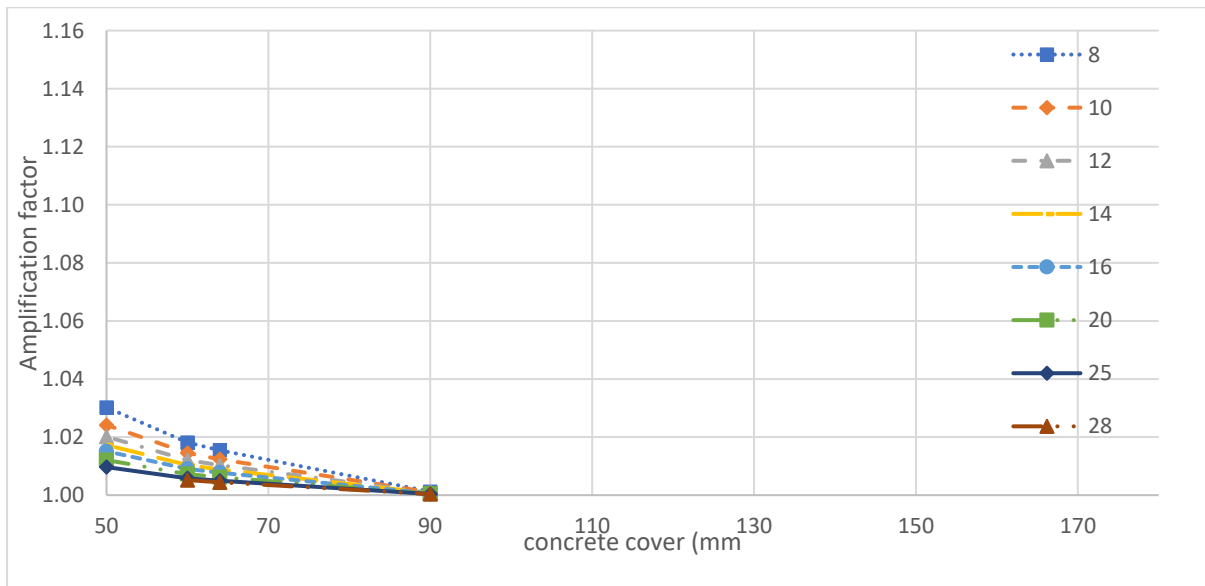


*Figure 4.9 Amplification factor for precast-side rebars at exposure time R30*

DIAMETER	CONCRETE COVER (MM)						
	30	40	50	60	90	120	130
8	1.10	1.090677	1.078976	1.07	1.03	1.00	1.00
10	1.08	1.072541	1.063181	1.05	1.02	1.00	1.00
12	1.07	1.060451	1.052651	1.04	1.02	1.00	1.00
14	1.06	1.051815	1.045129	1.04	1.02	1.00	1.00
16	1.05	1.045338	1.039488	1.03	1.01	1.00	1.00
20	1.04	1.036271	1.03159	1.03	1.01	1.00	1.00
25	1.03	1.029017	1.025272	1.02	1.01	1.00	1.00
28	1.03	1.025908	1.022565	1.02	1.01	1.00	1.00
32	1.03	1.022669	1.019744	1.02	1.01	1.00	1.00

Table 8 Amplification factor for precast-edge rebars at exposure time R30

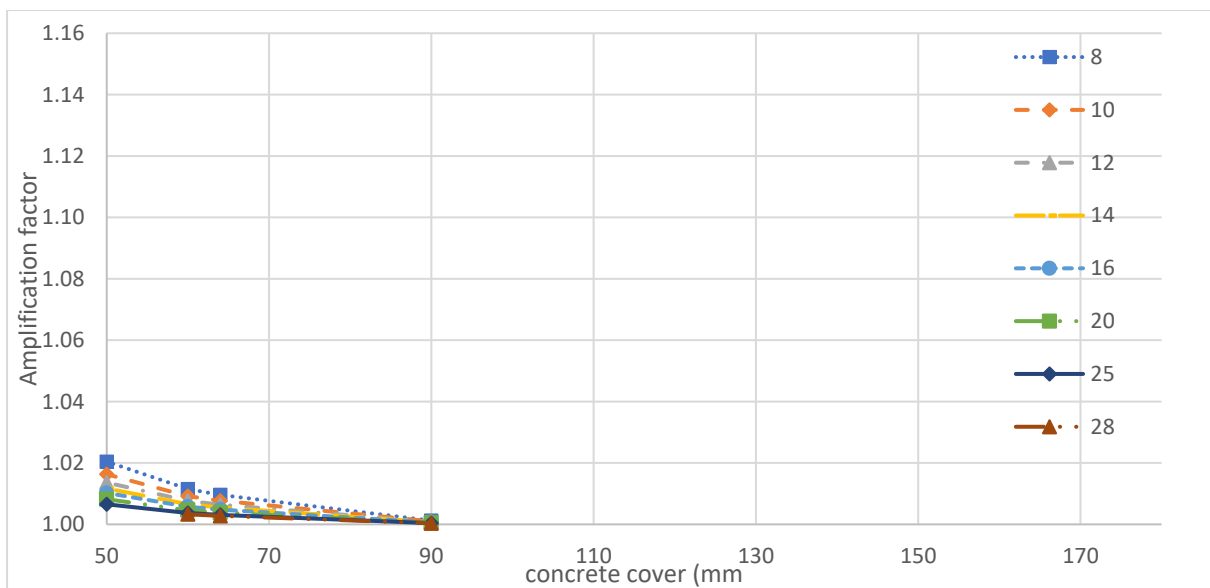


Figure 4.10 Amplification factor for precast-edge rebars at exposure time R30

Table 9 Amplification factor for precast-center rebars at exposure time R30

Diameter	concrete Cover (mm)					
	30	40	50	60	64	90
8	1.04	1.03	1.02	1.01	1.01	1.00
10	1.03	1.02	1.02	1.01	1.01	1.00
12	1.03	1.02	1.01	1.01	1.01	1.00
14	1.02	1.02	1.01	1.01	1.01	1.00
16	1.02	1.02	1.01	1.01	1.00	1.00
20		1.01	1.01	1.00	1.00	1.00
25			1.01	1.00	1.00	1.00
28				1.00	1.00	1.00

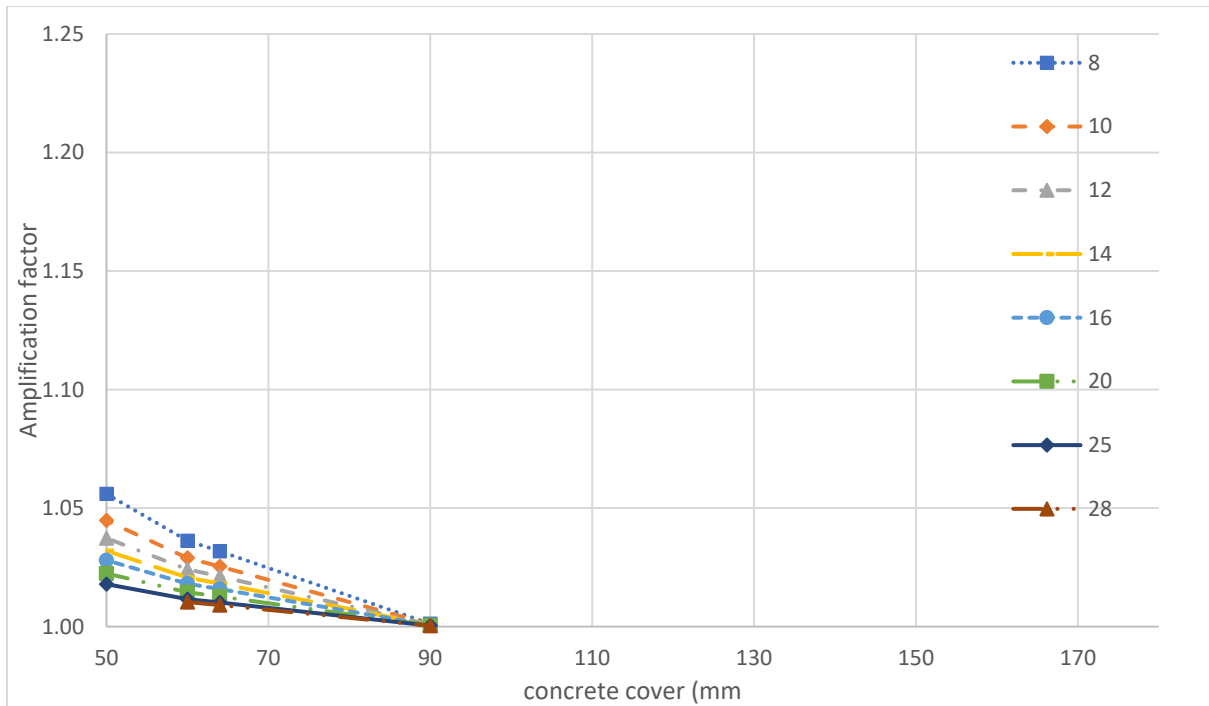


Figure 4.11 Amplification factor for precast-center rebars at exposure time R30

Table 10 Amplification factor for precast-center rebars at exposure time R30

Diameter	concrete Cover (mm)					
	30	40	50	60	64	90
8	1.09	1.07	1.06	1.04	1.03	1.00
10	1.07	1.06	1.04	1.03	1.03	1.00
12	1.06	1.05	1.04	1.02	1.02	1.00
14	1.05	1.04	1.03	1.02	1.02	1.00
16	1.05	1.04	1.03	1.02	1.02	1.00
20		1.03	1.02	1.01	1.01	1.00
25			1.02	1.01	1.01	1.00
28				1.01	1.01	1.00

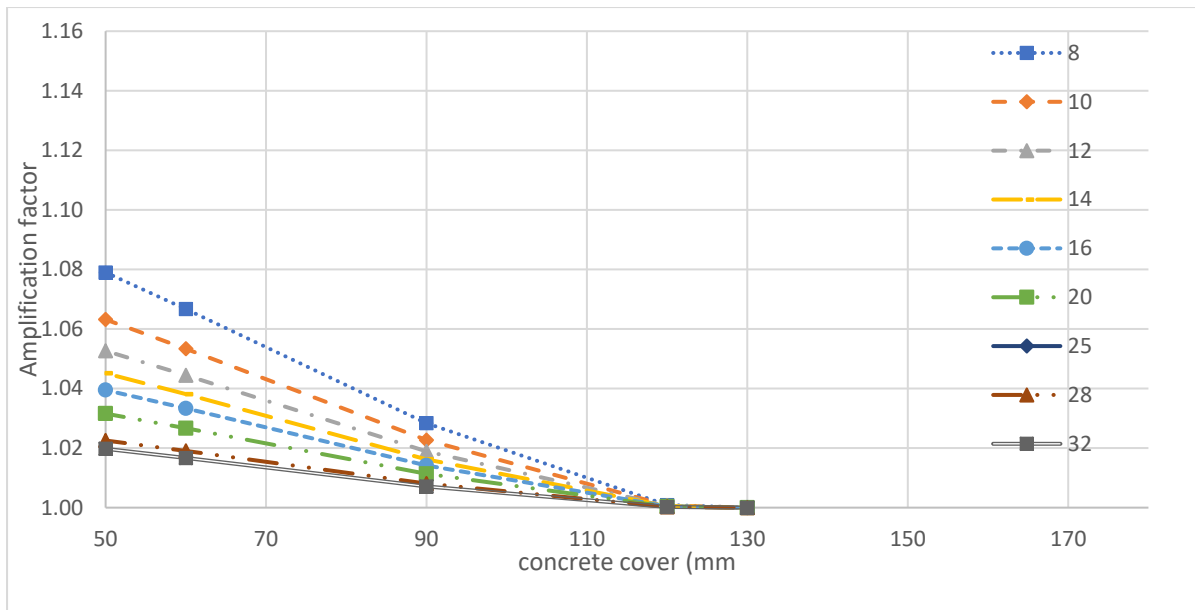


Figure 4.12 Amplification factor for precast-side rebars at exposure time R60

DIAMETE R	CONCRETE COVER (MM)									
	30	40	50	60	90	120	130	140	150	160
8	1.1	1.12	1.115	1.10	1.07	1.03	1.02	1.01	1.00	1.00
10	1.1	1.10	1.092	1.08	1.05	1.02	1.01	1.01	1.00	1.00
12	1.0	1.08	1.076	1.07	1.04	1.02	1.01	1.00	1.00	1.00
14	1.0	1.07	1.065	1.06	1.04	1.02	1.01	1.00	1.00	1.00
16	1.0	1.06	1.057	1.05	1.03	1.01	1.01	1.00	1.00	1.00
20		1.05	1.046	1.04	1.03	1.01	1.01	1.00	1.00	1.00
25			1.036	1.03	1.02	1.01	1.01	1.00	1.00	1.00
28				1.03	1.02	1.01	1.00	1.00	1.00	1.00
32					1.02	1.01	1.00	1.00	1.00	1.00

Table 11 Amplification factor for precast-side rebars at exposure time R60

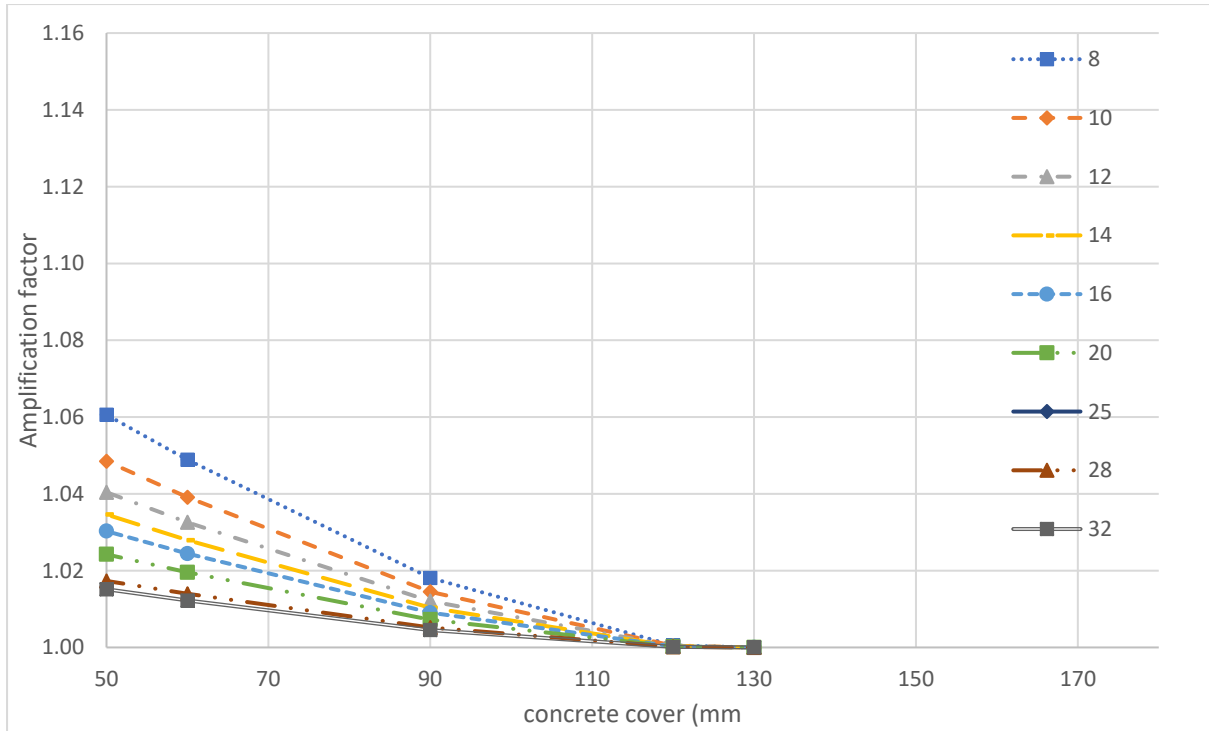


Figure 4.13 Amplification factor for precast-edge rebars at exposure time R60

Table 12 Amplification factor for precast-edge rebars at exposure time R60

Diameter	concrete Cover (mm)						
	30	40	50	60	90	120	130
8	1.09	1.072	1.06	1.05	1.02	1.00	1.00
10	1.07	1.058	1.048	1.04	1.01	1.00	1.00
12	1.06	1.048	1.040	1.03	1.01	1.00	1.00
14	1.05	1.041	1.034	1.03	1.01	1.00	1.00
16	1.04	1.036	1.030	1.02	1.01	1.00	1.00
20	1.03	1.029	1.024	1.02	1.01	1.00	1.00
25	1.03	1.023	1.019	1.02	1.01	1.00	1.00
28	1.02	1.020	1.017	1.01	1.01	1.00	1.00
32	1.02	1.018	1.015	1.01	1.00	1.00	1.00

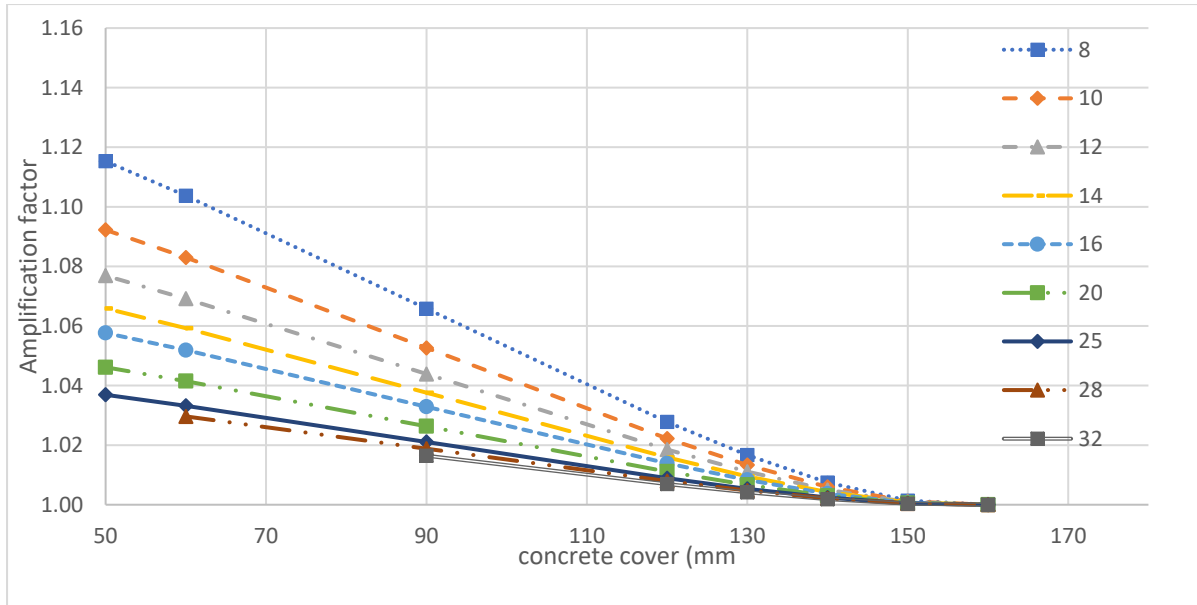


Figure 4.9 Amplification factor for precast-side rebars at exposure time R90

DIAMETER	CONCRETE COVER (MM)										
	30	40	50	60	90	120	130	140	150	160	180
8	1.17	1.16	1.15	1.13	1.10	1.06	1.05	1.03	1.02	1.012	1.00
10	1.14	1.12	1.12	1.11	1.08	1.05	1.04	1.03	1.02	1.010	1.00
12	1.11	1.10	1.10	1.09	1.07	1.04	1.03	1.02	1.01	1.008	1.00
14	1.10	1.09	1.08	1.08	1.06	1.03	1.03	1.02	1.01	1.007	1.00
16	1.09	1.08	1.07	1.07	1.05	1.03	1.02	1.02	1.01	1.006	1.00
20		1.06	1.06	1.05	1.04	1.02	1.02	1.01	1.01	1.005	1.00
25			1.05	1.04	1.03	1.02	1.01	1.01	1.01	1.004	1.00
28				1.04	1.03	1.02	1.01	1.01	1.01	1.004	1.00
32					1.02	1.01	1.01	1.01	1.01	1.003	1.00

Table 13 Amplification factor for precast-side rebars at exposure time R90

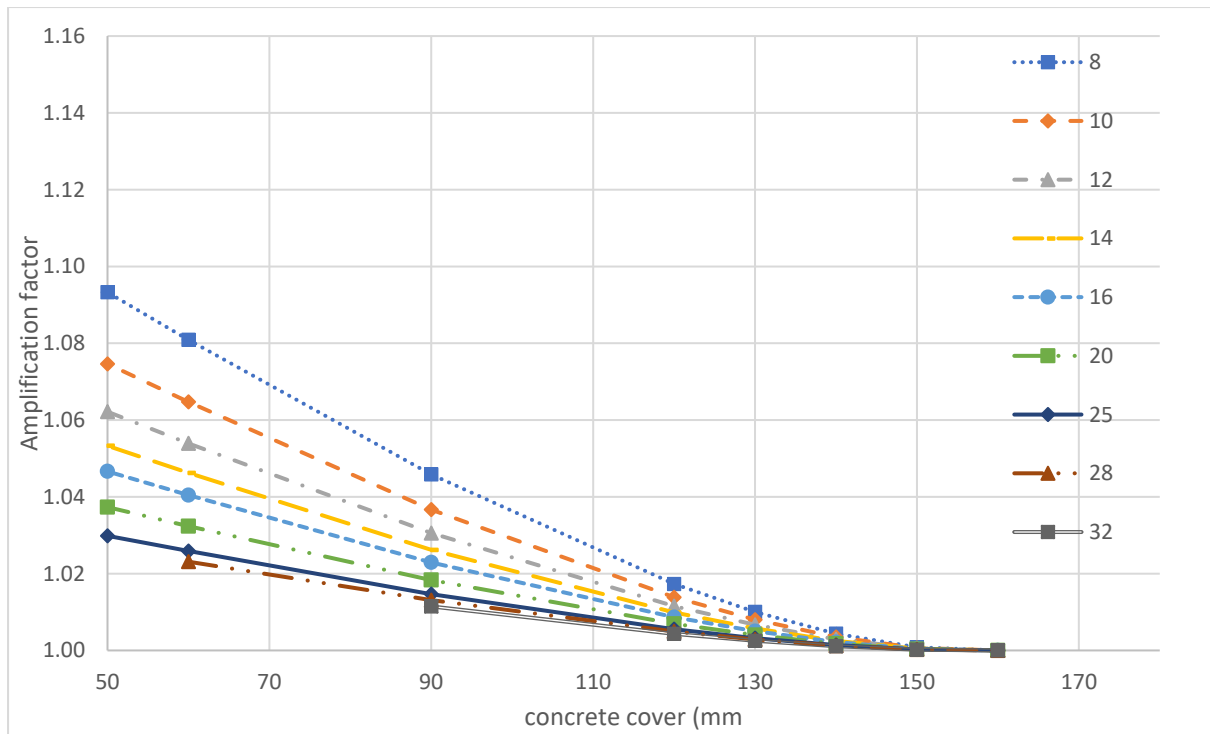


Figure 4.10 Amplification factor for precast-edge rebars at exposure time R90

Table 14 Amplification factor for precast-edge rebars at exposure time R90

Diameter <i>r</i>	concrete Cover (mm)									
	30	40	50	60	90	120	130	140	150	160
8	1.12	1.105761	1.093	1.08	1.05	1.02	1.01	1.00	1.00	1.00
10	1.09	1.084609	1.074	1.06	1.04	1.01	1.01	1.00	1.00	1.00
12	1.08	1.070507	1.062	1.05	1.03	1.01	1.01	1.00	1.00	1.00
14	1.07	1.060435	1.053	1.05	1.03	1.01	1.01	1.00	1.00	1.00
16	1.06	1.05288	1.046	1.04	1.02	1.01	1.01	1.00	1.00	1.00
20		1.042304	1.037	1.03	1.02	1.01	1.00	1.00	1.00	1.00
25			1.029	1.03	1.01	1.01	1.00	1.00	1.00	1.00
28				1.02	1.01	1.00	1.00	1.00	1.00	1.00
32					1.01	1.00	1.00	1.00	1.00	1.00

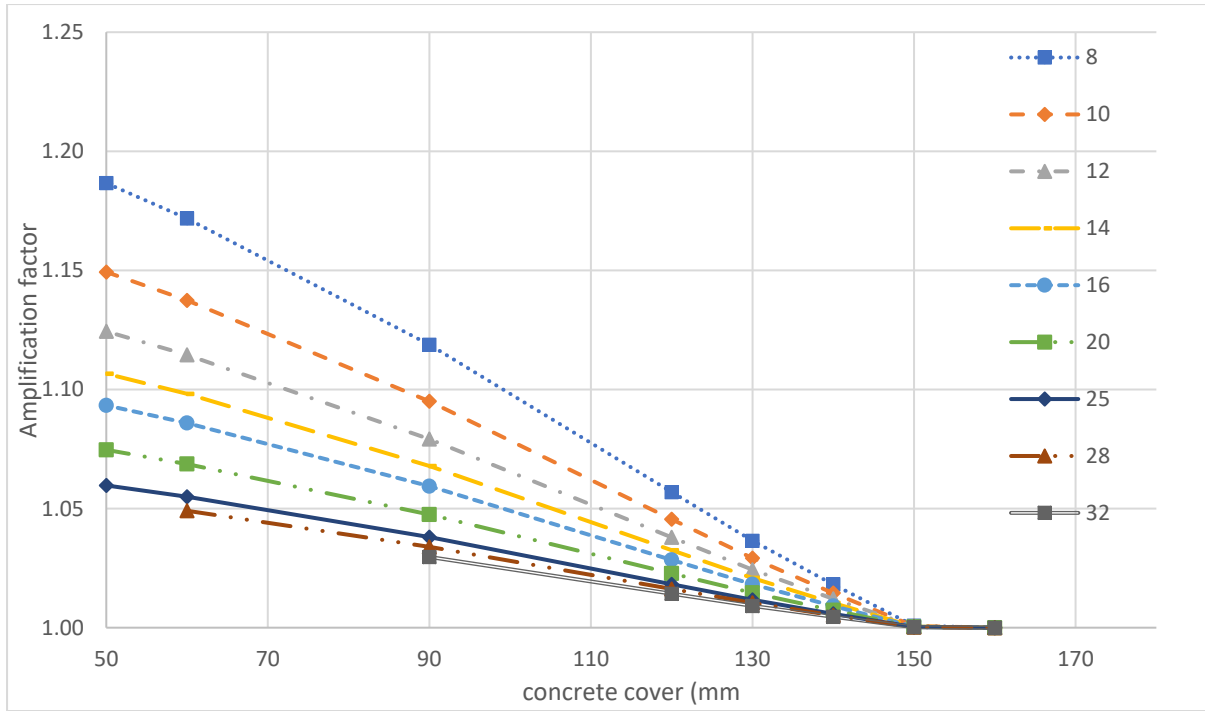


Figure 4.12 Amplification factor for precast-center rebars at exposure time R90

Table 15 Amplification factor for precast-center rebars at exposure time R90

Diameter <i>r</i>	concrete Cover (mm)									
	30	40	50	60	90	120	130	140	150	160
8	1.21	1.1998	1.18661	1.17	1.12	1.06	1.04	1.02	1.00	1.00
10	1.17	1.15984	1.149288	1.14	1.10	1.05	1.03	1.01	1.00	1.00
12	1.14	1.1332	1.124407	1.11	1.08	1.04	1.02	1.01	1.00	1.00
14	1.12	1.114171	1.106634	1.10	1.07	1.03	1.02	1.01	1.00	1.00
16	1.11	1.0999	1.093305	1.09	1.06	1.03	1.02	1.01	1.00	1.00
20		1.07992	1.074644	1.07	1.05	1.02	1.01	1.01	1.00	1.00
25			1.059715	1.05	1.04	1.02	1.01	1.01	1.00	1.00
28				1.05	1.03	1.02	1.01	1.01	1.00	1.00
32					1.03	1.01	1.01	1.00	1.00	1.00

From the above results it can be seen that, for a certain exposure time, amplification factors for smaller bar diameters are lower as compared to that for larger diameters. This is an obvious consequence of the basic anchorage length formula that states that length is directly proportional to the bar diameter.

Further, all the graphs converge at amplification factor 1, however, the value of edge distance at which it is achieved increases as we increase the exposure time.

These results are for pre-cast side case. Pre-cast edge and center follows the same trend with different starting values.

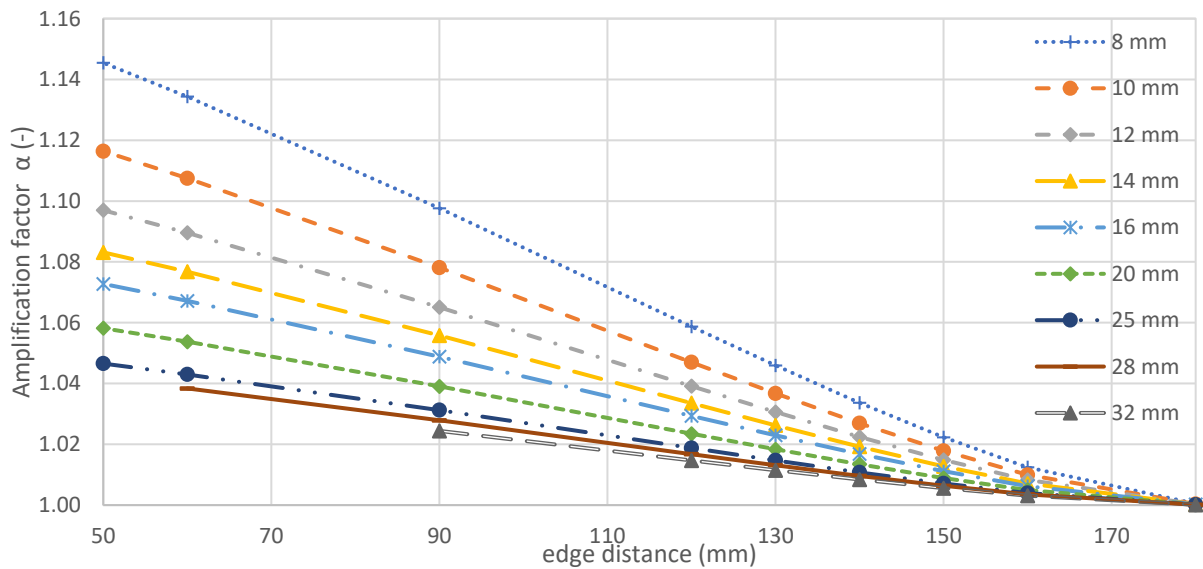


Figure 4.13 Amplification factor for precast-side rebars at exposure time R120

Table 16 Amplification factor for precast-side rebars at exposure time R120

Diameter	concrete Cover (mm)										
	30	40	50	60	90	120	130	140	150	160	180
8	1.17	1.16	1.15	1.13	1.10	1.06	1.05	1.03	1.02	1.012	1.00
10	1.14	1.12	1.12	1.11	1.08	1.05	1.04	1.03	1.02	1.010	1.00
12	1.11	1.10	1.10	1.09	1.07	1.04	1.03	1.02	1.01	1.008	1.00
14	1.10	1.09	1.08	1.08	1.06	1.03	1.03	1.02	1.01	1.007	1.00
16	1.09	1.08	1.07	1.07	1.05	1.03	1.02	1.02	1.01	1.006	1.00
20		1.06	1.06	1.05	1.04	1.02	1.02	1.01	1.01	1.005	1.00
25			1.05	1.04	1.03	1.02	1.01	1.01	1.01	1.004	1.00
28				1.04	1.03	1.02	1.01	1.01	1.01	1.004	1.00
32					1.02	1.01	1.01	1.01	1.01	1.003	1.00

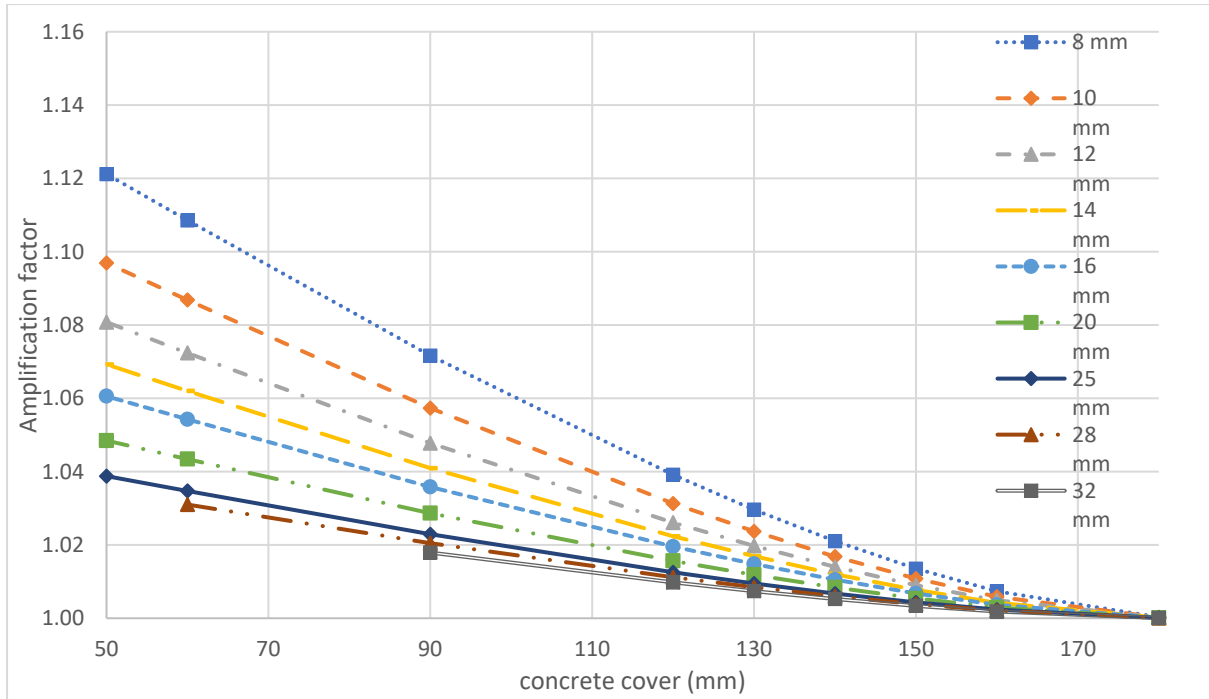


Figure 4.14 Amplification factor for precast-edge rebars at exposure time R120

Table 17 Amplification factor for precast-edge rebars at exposure time R120

	concrete Cover (mm)										
<b>Diameter</b>	<b>30</b>	<b>40</b>	<b>50</b>	<b>60</b>	<b>90</b>	<b>120</b>	<b>130</b>	<b>140</b>	<b>150</b>	<b>160</b>	<b>180</b>
8	1.15	1.13	1.12	1.11	1.07	1.04	1.03	1.02	1.01	1.007	1.00
10	1.12	1.11	1.10	1.09	1.06	1.03	1.02	1.02	1.01	1.006	1.00
12	1.10	1.09	1.08	1.07	1.05	1.03	1.02	1.01	1.01	1.005	1.00
14	1.08	1.08	1.07	1.06	1.04	1.02	1.02	1.01	1.01	1.004	1.00
16	1.07	1.07	1.06	1.05	1.04	1.02	1.01	1.01	1.01	1.004	1.00
20		1.05	1.05	1.04	1.03	1.02	1.01	1.01	1.01	1.003	1.00
25			1.04	1.03	1.02	1.01	1.01	1.01	1.00	1.002	1.00
28				1.03	1.02	1.01	1.01	1.01	1.00	1.002	1.00
32					1.02	1.01	1.01	1.01	1.00	1.002	1.00

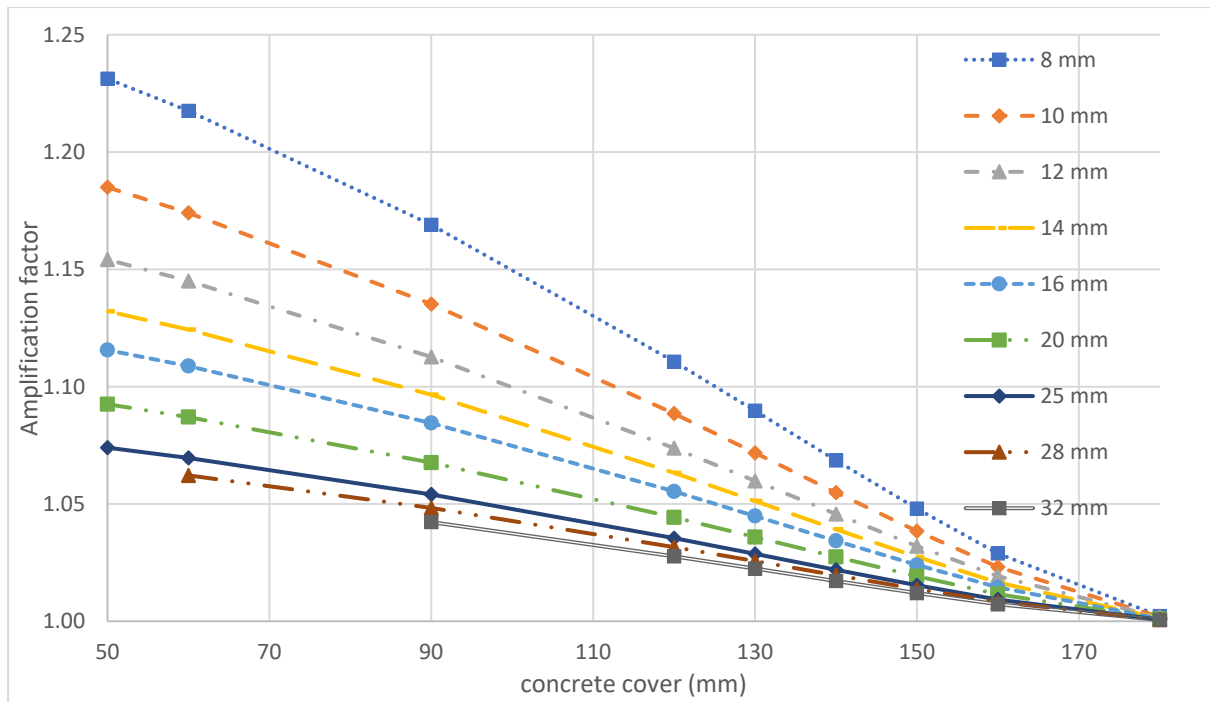


Figure 4.15 Amplification factor for precast-center rebars at exposure time R120

Table 18 Amplification factor for precast-center rebars at exposure time R120

Diameter	concrete Cover (mm)										
	30	40	50	60	90	120	130	140	150	160	180
8	1.25	1.24	1.23	1.22	1.17	1.11	1.09	1.07	1.05	1.029	1.00
10	1.20	1.19	1.18	1.17	1.14	1.09	1.07	1.05	1.04	1.023	1.00
12	1.17	1.16	1.15	1.15	1.11	1.07	1.06	1.05	1.03	1.019	1.00
14	1.15	1.14	1.13	1.12	1.10	1.06	1.05	1.04	1.03	1.017	1.00
16	1.13	1.12	1.12	1.11	1.08	1.06	1.04	1.03	1.02	1.014	1.00
20		1.10	1.09	1.09	1.07	1.04	1.04	1.03	1.02	1.012	1.00
25			1.07	1.07	1.05	1.04	1.03	1.02	1.02	1.009	1.00
28				1.06	1.05	1.03	1.03	1.02	1.01	1.008	1.00
32					1.04	1.03	1.02	1.02	1.01	1.007	1.00

## 4.5 Amplification factor for Laps

Unlike for anchorage at beam-column connection, amplification factor for laps does not depend on the bar diameter, rather it only depends on the edge distance and exposure time. Hence, Figure 12 shows amplification factor for all the range of bar diameter. Below a certain value of edge distance, concrete is completely damaged by fire, thus finding an amplification factor is not possible.

However, this is more sensitive than the previous case, since for edge distance values less than 30 mm reduction factor drops to zero for 30 minute exposure time.

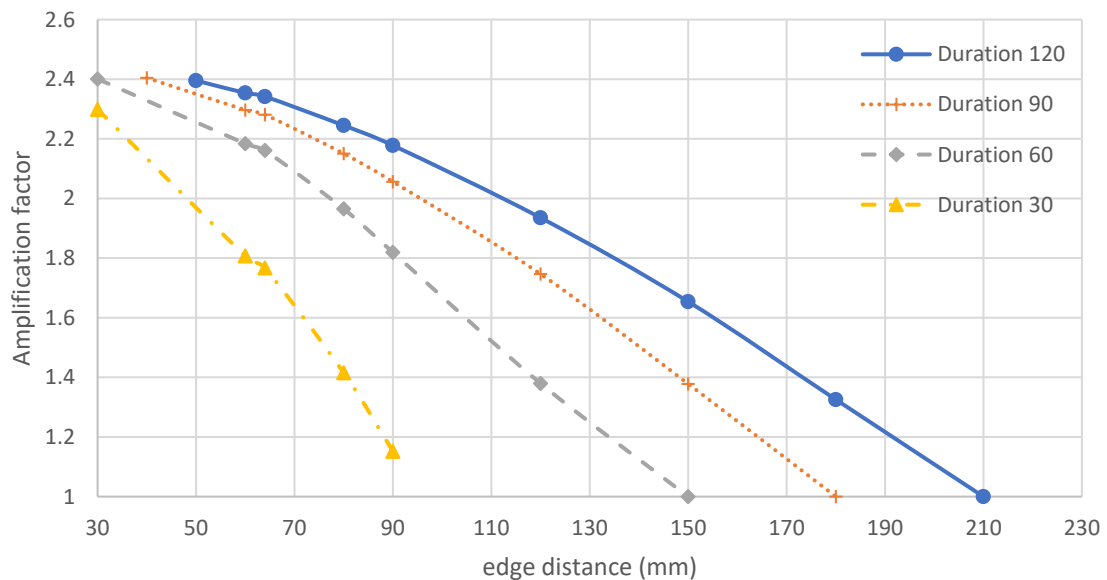


*Figure 4.15 Amplification factor for laps*

In this case, there exists a lower bound of edge distance, the value of which varies for different exposure time. Beyond this value, bond strength drops to zero and hence amplification factor cannot be calculated. This bound increases for higher exposure times due to the temperature growth within the element.

# Conclusion

This thesis discusses the performance of pre and post installed anchorage at beam column connection and laps under a fire event. An analytical investigation is carried out to quantify the degradation effects in such scenarios and a solution to accommodate them is presented, that was to propose an amplification factor that can be multiplied with basic embedded length to get length increment. Length increment was computed to compensate the amount of loss for the bond strength during fire situation.

The proposed scheme uses experimental bond strength reduction curves (normalized results) from previous researches of specimens covering various cases of rebar position and nature of bar installment (pre-cast or post-installed). Given the general behavior of bond strength vs temperature for different cases is known through experiments, case specific bond behavior can be computed using heat transfer simulation results for a certain geometric configuration. Subsequently, amplification factor can be obtained for different cases of rebar position (being center, side and edge) and sizes (less than 32mm bar diameters, that to ensure the uniformity of bond strength across the embedded length), which is to be multiplied with basic anchorage length to find incremented length that ensures safety and can sustain the applied load for different requirements of exposure time.

Additionally, same scheme is employed also to find the amplification factor in case of laps and the results are reported. Amplification factor for laps was a sensitive case since there exist a lower bound for edge distance, which differs for different cases of exposure time. Moreover, amplification factor for laps was simply the inverse of reduction factor for given a temperature at that point, this is due to the fact that temperature across the embedded length of lap was constant.

Three different amplification factors are considered for anchorages at beam column connection that are: (i) a post-installed rebar far from edges ('post-installed center'), (ii) a pre-cast rebar far from edges ('pre-cast center'), (iii) a pre-cast rebar closed to an edge ('pre-cast side') and (iii) a pre-cast rebar closed to an edge ('pre-cast edge'). For laps, the only case dealt here is rebar far from edges (pre-cast center) and also for post-installed the only case dealt was "center", due to the fact that only available reduction curve for post-installed was for case of center rebar position.

However, it is noticed that such amplification factor depends not only on the exposure time, but on bar diameter and edge distance, as well. Precisely, it decreases non linearly with increasing bar diameter. By increasing edge distance, amplification factor gradually converges to one for all cases, however, the specific edge distance for which it is achieved depends upon the exposure time, as this value increase for increasing exposure time. Further, degradation effects here are applied only on concrete and due to this reason, in case of center position the entire contribution of bond strength comes from adjacent concrete, thus, the lack of transversal reinforcement for the case of 'center' rebar position results in higher values of the amplification factor. In contrast, there is a contribution of transversal stirrups in case of edge and side positions tends to lower the amplification factor for these cases.

Comparatively, an interesting observation is seen for post installed bars, where amplification factor raises slowly as temperature builds up in the element. This follows the trend of bond strength reduction curve for post installed bars. For laps, given a certain value of edge distance, amplification factor is inversely related to the reduction factor  $\chi(T(y))$ . However, there exist a lower bound for rebar position in this case as, at values of edge distance smaller than this value, bond strength is completely lost. This lower bound may vary for different exposure times.

A remarkable advantage of this scheme is that it is general and is not specific for a certain configuration. Hence, despite the reduced number of cases presented, amplification factors can be obtained for various geometric configurations using the proposed approach with the only edition to temperature profiles that can be achieved through heat transfer analysis.

This would help in developing a method in the future that can be useful to designers for evaluating the anchorage length and lap splices under fire scenarios. It is remarked how the evaluation of the amplification factors is carried out by assuming that the value of force to be transferred from steel to concrete is constant; hence it does not account for possible reductions due to the decay of steel properties as an effect of temperature or to different partial safety factors to be accounted for design under a fire event.

## References:

1. Abrams, M. S. (1971). Compressive strength of concrete at temperatures to 1600F. *Special Publication*, 25, 33-58.
2. Agnoletti, Consiglio, Muciaccia, Bosnjak, & Sharma. (2019). Effects of elevated temperatures and of loading procedures on the bond performance of reinforcement in PROTECT 2019: 7th International Colloquium on Performance, Protection and Strengthening of Structures Under Extreme Loading and Events, Whistler, BC, Canada, September 16-17, 2019 concrete, In: *Proceedings of the Ninth International Conference on Concrete Under Severe Conditions-Environment & Loading (CONSEC 2019)*, in press
3. Aslani, F., & Samali, B. (2013). Predicting the bond between concrete and reinforcing steel at elevated temperatures. *Structural Engineering and Mechanics*, 48(5), 643-660.
4. Bingöl, A. F., & Gül, R. (2009). Residual bond strength between steel bars and concrete after elevated temperatures. *Fire Safety Journal*, 44(6), 854-859.
5. Castillo, C. (1987). Effect of transient high temperature on high-strength concrete (Doctoral dissertation, Rice University).
6. CEB-FIP MC-90, 1990. CEB-FIP Model Code, Final Draft, Committee Euro-International du Beton, Bulletin n. 213/214, Lausanne, Switzerland.
7. Concrete Society (1990). Assessment and repair of fire-damaged concrete structures. Technical Report (33). Camberley, UK.
8. EN, B. (2004). 1-2: 2004 Eurocode 2: Design of concrete structures-Part 1-2: General rules-Structural fire design. European Standards, London.
9. Esfahani, M. R., Rangan, B. V., 2000. Influence of transverse reinforcement on bond strength of tensile splices. *Cement and Concrete Composites* 22, 159-163.

10. Ferguson, P. M., 1958. Reinforced concrete fundamentals with emphasis on ultimate strength. John Wiley and Sons, Inc., New York.
11. FIB MC-10, 2012. Model Code 2010, Final draft. International Federation for Structural Concrete (fib- fédération internationale du béton), Lausanne, Switzerland.
12. FIB Bulletin-10-2000, 2000. Bond of reinforcement in concrete. FIB Bulletin No. 10, International Federation for Structural Concrete (fib- fédération internationale du béton), Lausanne, Switzerland.
13. Fanella, D. A., 2011. Reinforced concrete structures: Analysis and design, McGraw- Hill companies, USA.
14. Ferguson, P. M., 1977. Small bar spacing or cover - a bond problem for the designer, ACI Journal 74(9), 435-439.
15. Gambarova, P. G., Rosati, G. P., Schumm, C.E., 1996. An elasto-cohesive model for steel-concrete bond, in: Bazánt, Z., Bittnar, Z., Jirasek, M., Mazars, J. (Eds.), Proc. Europe- US workshop on fracture and damage in quasibrittle structure, Prague (Czech Republic), pp 557-566.
16. Harada, T., Takeda, J., Yamane, S., & Furumura, F. (1972). Strength, elasticity and thermal properties of concrete subjected to elevated temperatures. Special Publication, 34, 377-406.
17. ISO 834-1, Fire-resistance tests, Elements of building construction, Part 1: General requirements
18. Luccioni, Figueroa, & Danesi. (2003). Thermo-mechanic modal for concrete exposed to elevated temperatures. Eng struct , 25, 729-42
19. Lahouar, Caron, Pinoteau, & Gilles. (2017). Mechanical behaviour of adhesive anchors under high temperature exposure: experimental investigation. International Journal of adhesion and adhesives, 78, 200-211.

20. Muciaccia, Consiglio, & Rosati. (2016). Behaviour and design of post-installed rebar connections under temperature. *Key Engineering Material*, 711, 783-790
21. Nilson, A. H., Darwin, D., Dolan, C. W., 2004. *Design of Concrete Structures*, thirteenth ed. The McGraw-Hill Companies, New York.
22. N. Pinoteau, P. Pimienta, T. Guillet, P. Rivillon and S. Rémond, Effect of heating rate on bond failure of rebars into concrete using polymer adhesives to simulate exposure to fire. *International Journal of Adhesion and Adhesives*, 31 (2011), pp. 851–861.
23. Park, R., Paulay, T., 1975. *Reinforced Concrete Structures*, second ed. Wiley-Interscience, New York.
24. Phan, L. T. (1996). *Fire performance of high-strength concrete: A report of the state-of-the-art*. US Department of Commerce, Technology Administration, National Institute of Standards and Technology, Office of Applied Economics, Building and Fire Research Laboratory.
25. Reis J. (2012). Effects of temperature on the mechanical properties of polymer mortars. *Marter res*, 15(4), 469-9.
26. Tepfers, R., 1973. A theory of bond applied to overlapped tensile reinforcement splices for deformed bars. Division of Concrete Structures, Chalmers University of Technology, Goteborg, Sweden, 73:2.
27. Tepfers, R., 1979. Cracking of concrete cover along anchored deformed reinforcing bars. *Magazine of Concrete Research* 31(106), 3-12.
28. Tepfers, R., 1982. Lapped tensile reinforcement splices. *Journal of Structural Division* 108(1), 283-301.
29. Tepfers, R., Olsson, P.A., 1992. Ring test for evaluation of bond properties of reinforcing bars. *Proceedings of International Conference on "Bond in Concrete: from Research to Practice"*, CEB-RTU (Riga Technical University), Riga (Latvia), 1.89-1.99.

30. Thelandersson, S. (1972). Effect of high temperatures on tensile strength of concrete.  
Bulletines of Division of Structural Mechanics and Concrete Construction, Bulletin 26.
31. Xiao, J., & König, G. (2004). Study on concrete at high temperature in China—an overview.  
Fire safety journal, 39(1), 89-103.

## Annex A

### MATLAB CODE:

%Inputs

d = [8 10 12 14 16 20 25 28 32 ]; %diameter values

Xi = [1.00 0.68 0.72 0.57 0.53 0.42 0.39 ]; % reduction factor

Ti = [30 47.2 63.2 108 118.8 511.8 523.1 ]; %corresponding temperature

R = [30 60 90 120 ]; % exposure time [min]

yi = 50; %concrete cover [m]

fbd20 = 2.69; % design bond strength at ambient temperature

Amp = zeros(length(d),length(R));

for i=1:length(d)

di = d(i);

for j=1:length(R)

Rj = R(j) ;

%solution

fyd = 391.3043478;

ld\_20 = (di/4)\*(fyd/fbd20);

%Pick data corresponding to Rvalue by loading temperature data annex -B

if (Rj == 30)

X=x30;

Y=y30;

T=T30;

elseif (Rj == 60)

X=x60;

```

Y=y60;

T=T60;

elseif (Rj == 90)

X=x90;

Y=y90;

T=T90;

else

X=x120;

Y=y120;

T=T120;

end

if yi > max(Y)

ld = ld_20

else

m = find( Y == yi);

x_n = X(m, :);

t_n = T(m, :);

v = find( t_n == 20);

ty = t_n(:, 1:v);

xy = x_n(:, 1:v);

xy = xy';

func1 = fit(Ti,Xi,'power2');

func1

Ti1= [Ti(1):1:Ti(end)];

```

```

vfunc1 = func1(Ti1);

figure(1)

plot(Ti1,vfunc1);

title('Reduction curve');

hold on

scatter(Ti,Xi,'filled');

hold off

legend('Approximated curve','Test data');

xlabel('Temperature °C');

ylabel('Reduction factor');

Xt = func1(ty);

Xt1 = func1(Ti(end));

Xt(Xt>1)=1;

Xt(Xt<Xt1)=0;

jh = find (Xt ==1);

Xt = Xt(1:jh(1),:);

fbd_T = fbd20.*Xt;

v=find(fbd_T==0);

fbd_T(v)=[];

xy(v)=[];

gh = find (fbd_T == fbd20);

xy = xy(1:gh,:);

func2 = fit (xy,fbd_T,'power2' );

func2

```

```

xy1 = [xy(1):xy(end)+1];

vfunc2 = func2(xy1);

figure(2)

plot(xy1,vfunc2);

%title('fbd(T) distribution along the embedded depth');

hold on

scatter(xy,fbd_T,'filled');

%hold off

legend('Approximated curve','Node Temperature');

xlabel('Embedded depth = x(mm)');

ylabel('fbd(T)');

coefvals = coeffvalues(func2);

a = coefvals(1);

b = coefvals(2);

c = coefvals(3);

C=pi*di;

F=fbd20*C*ld_20;

syms x y

f = int(a*x^b + c, [xy1(1) xy1(end)]);

A1 = (fbd20*(xy1(end)-xy1(1)))-f;

A2 = fbd20*xy(1);

add = (A1+A2)/fbd20;

ld_T = ld_20+add;

format short

```

ld\_20

ld\_T = vpa(ld\_T,6)

Amp(i,j) = vpa(ld\_T/ld\_20, 6);

end

end

end

Amp

## Annex -B

### Temperature Data

% R30

y30 =[30 40 50 60 64 80 90]; % edge distance(concrete cover) in [mm]

% distance from exposed surface along the embedded length [mm]

%rows corresponds to concrete cover given in y30 vector , i.e first row is for 30 mm cover

x30 = [0.001 3.33 6.67 10.00 13.33 16.67 20.00 23.33 26.67 30.00

33.33 36.67 40.00 43.33 46.67 50.00 53.33 56.67 60.00 63.33 66.67

70.00 73.33 76.67 80.00 ;

0.001 3.33 6.67 10.00 13.33 16.67 20.00 23.33 26.67 30.00 33.33

36.67 40.00 43.33 46.67 50.00 53.33 56.67 60.00 63.33 66.67 70.00

74.00 0.00 0.00 ;

0.001 3.33 6.67 10.00 13.33 16.67 20.00 23.33 26.67 30.00 33.33

36.67 40.00 43.33 46.67 50.00 53.33 56.67 60.00 63.33 66.67 0.00

0.00 0.00 0.00 ;

0.001 3.33 6.67 10.00 13.33 16.67 20.00 23.33 26.67 30.00 33.33

36.67 40.00 43.33 46.67 50.00 53.33 56.67 0.00 0.00 0.00 0.00

0.00 0.00 0.00 ;

0.001 3.33 6.67 10.00 13.33 16.67 20.00 23.33 26.67 30.00 33.33

36.67 40.00 43.33 46.67 50.00 53.33 56.67 0.00 0.00 0.00 0.00

0.00 0.00 0.00 ;

0.001 3.33333 6.66667 10 13.3333 16.6667 20 23.3333 26.6667 30 0 0 0 0 0

0 0 0 0 0 0 0 0 0 ;

0.001 3.33 6.67 10.00 13.33 16.67 20.00 23.33 26.67 30.00 0.00

0.00 0.00 0.00 0.00 0.00 0.00 0.00 0.00 0.00 0.00 0.00

0.00 0.00 0.00

];

% temperature at the axise along the embedded length

%similarly each row corresponds to certain concrete cover

T30 = [206.492 195.827 185.161 173.563 160.098 146.632 135.406 125.33 115.23 104.084

95.0659 87.6729 79.0175 71.2012 65.2206 58.5469 52.2532 47.5364 42.4597 37.6022

33.9809

30.1689 26.5343 23.8183 20 ;

143.028 136.277 129.527 122.241 114.053 105.865 98.8567 92.0776 85.4437 79.8292

73.0392

65.9482 61.0371 55.7897 49.8119 45.7278 41.5712 36.8544 33.5093 30.234 26.6127

24.0258

20 0 0 ;

100.195 95.9938 91.7925 87.1551 81.8584 76.5618 72.2307 67.8352 63.4245 57.8542

53.9118

50.0745 45.3552 41.6483 38.3632 34.5974 31.3625 28.6013 25.6415 23.0536 20 0 0 0

0 ;

71.7047 68.5676 65.4306 62.0967 58.47 54.8434 51.738 48.6333 45.5286 42.4234 39.3181

36.167 33.6219 30.8619 27.8892 25.6692 23.4492 20 0 0 0 0 0 ;

62.543 62.113 59.5642 56.5854 53.2639 50.6485 48.164 45.3534 42.4263 39.4004 36.6757

```

34.2954 31.7825 29.1954 26.7005 24.6997 22.5758 20 0 0 0 0 0 0 ;
33.2738 32.1527 31.0315 29.7082 28.084 26.4598 25.0782 23.7558 22.3918 20 0 0 0
0 0 0 0 0 0 0 0 0 0 ;
22.4752 21.721 20.9667 20 0 0 0 0 0 0 0 0 0 0 0 0 0 0
0 0 0 0 0 0
];
% R60
y60 = [30 40 50 60 64 80 90 120 130 ];
x60 = [0.001 3.33 6.67 10.00 13.33 16.67 20.00 23.33 26.67 30.00
33.33 36.67 40.00 43.33 46.67 50.00 53.33 56.67 60.00 63.33 66.67
70.00 73.33 76.67 80.00 83.33 86.67 90.00 93.33 96.67 100.00 103.33
106.67 110.00 113.33 116.67 120.00 123.33 126.67 ;
0.001 3.33 6.67 10.00 13.33 16.67 20.00 23.33 26.67 30.00 33.33
36.67 40.00 43.33 46.67 50.00 53.33 56.67 60.00 63.33 66.67 70.00
73.33 76.67 80.00 83.33 86.67 90.00 93.33 96.67 100.00 103.33 106.67
110.00 113.33 116.67 120.00 123.33 0.00 ;
0.001 3.33 6.67 10.00 13.33 16.67 20.00 23.33 26.67 30.00 33.33
36.67 40.00 43.33 46.67 50.00 53.33 56.67 60.00 63.33 66.67 70.00
73.33 76.67 80.00 83.33 86.67 90.00 93.33 96.67 100.00 103.33 106.67
110.00 113.33 116.67 0.00 0.00 0.00 ;
0.001 3.33 6.67 10.00 13.33 16.67 20.00 23.33 26.67 30.00 33.33
36.67 40.00 43.33 46.67 50.00 53.33 56.67 60.00 63.33 66.67 70.00
73.33 76.67 80.00 83.33 86.67 90.00 93.33 96.67 100.00 103.33 106.67
110.00 113.33 0.00 0.00 0.00 0.00 ;
0.001 3.33 6.67 10.00 13.33 16.67 20.00 23.33 26.67 30.00 33.33
36.67 40.00 43.33 46.67 50.00 53.33 56.67 60.00 63.33 66.67 70.00
73.33 76.67 80.00 83.33 86.67 90.00 93.33 96.67 100.00 103.33 106.67
110.00 113.33 0.00 0.00 0.00 0.00 ;
0.001 3.33 6.67 10.00 13.33 16.67 20.00 23.33 26.67 30.00 33.33
36.67 40.00 43.33 46.67 50.00 53.33 56.67 60.00 63.33 66.67 70.00
73.33 76.67 80.00 83.33 86.67 90.00 93.33 96.67 0.00 0.00 0.00
0.00 0.00 0.00 0.00 0.00 0.00 ;
0.001 3.33 6.67 10.00 13.33 16.67 20.00 23.33 26.67 30.00 33.33
36.67 40.00 43.33 46.67 50.00 53.33 56.67 60.00 63.33 66.67 70.00
73.33 76.67 80.00 83.33 86.67 0.00 0.00 0.00 0.00 0.00 0.00
0.00 0.00 0.00 0.00 0.00 0.00 ;
0.001 3.33 6.67 10.00 13.33 16.67 20.00 23.33 26.67 30.00 33.33
36.67 40.00 43.33 46.67 0.00 0.00 0.00 0.00 0.00 0.00 0.00
0.00 0.00 0.00 0.00 0.00 0.00 0.00 0.00 0.00 0.00 0.00
0.00 0.00 0.00 0.00 0.00 0.00 0.00 0.00 0.00 0.00 0.00
0.00 0.00 0.00 0.00 0.00 0.00
];
T60 = [337.804 324.162 310.52 295.826 279.024 262.222 246.994 232.569 218.115 202.433
189.162 177.718 164.354 152.196 142.673 132.09 122.088 114.5 106.292 98.3257 91.9338

```

85.2557 78.7869 73.4639 67.9514 62.6209 58.2255 53.7272 49.3857 45.7892 42.143  
38.6301  
35.7128 32.7784 29.9563 27.6118 25.2699 23.0215 20 ;  
260.391 250.526 240.66 230.139 218.513 206.886 195.953 185.035 174.35 165.3 154.674  
143.656 135.672 127.204 117.686 111.039 104.284 96.6967 90.7787 84.9357 78.5438  
73.4864  
68.5062 63.1833 58.9359 54.7552 50.3598 46.8354 43.3684 39.7719 36.8793 34.0355  
31.1183  
28.7696 26.4621 24.1176 22.2299 20 0 ;  
199.952 193.211 186.47 178.998 170.42 161.843 154.667 147.37 140.051 131.059 124.474  
118.045 110.338 104.163 98.6225 92.4166 86.783 81.7112 76.3421 71.3909 66.9246  
62.2881  
58.0632 54.2204 50.2686 46.7106 43.4645 40.1468 37.1875 34.4844 31.7354 29.3043  
27.0825  
24.8325 22.8578 20 0 0 0 ;  
155.921 150.517 145.113 139.443 133.378 127.313 122.058 116.798 111.538 106.229  
100.915  
95.4185 90.7276 85.7904 80.6133 76.3089 72.0045 67.4169 63.5055 59.5941 55.6666  
52.2128  
48.7591 45.4064 42.4283 39.4502 36.5943 34.0746 31.5549 29.1607 27.0615 24.9623  
22.9832  
21.2572 20 0 0 0 0 ;  
141.147 140.545 136.059 130.972 125.327 120.825 116.525 111.753 106.813 101.692  
96.8524  
92.4419 87.8525 83.1631 78.5917 74.5986 70.4119 66.2251 62.7131 58.8221 54.9477  
51.9186  
48.4806 45.0844 42.423 39.4688 36.5461 34.2491 31.748 29.277 27.3339 25.248 23.1897  
21.5706 20 0 0 0 0 ;  
93.2642 90.8641 88.4641 85.7761 82.6597 79.5432 76.6516 73.8148 70.9124 67.7397  
64.567  
61.6086 58.7804 55.9522 53.0417 50.1218 47.4033 44.9185 42.327 39.7356 37.512 35.2118  
32.9115 30.9311 28.902 26.873 25.1782 23.4235 21.6688 20 0 0 0 0 0 0  
0 0 ;  
73.0932 71.2124 69.3316 67.2493 64.8671 62.4849 60.2976 58.1578 55.9592 53.534  
51.1088  
48.8483 46.6941 44.5399 42.2978 40.0502 37.8997 35.9548 34.0099 32.0385 30.0635  
28.3481  
26.6783 24.963 23.3574 21.9192 20 0 0 0 0 0 0 0 0 0 0 ;  
33.9949 33.1238 32.2526 31.2933 30.2028 29.1123 28.1475 27.2135 26.2473 25.1575  
24.0676  
23.0716 22.1362 21.1999 20 0 0 0 0 0 0 0 0 0 0 0 0  
0 0 0 0 0 0 0 0 ;  
25.881 25.2296 24.5783 23.8551 23.025 22.1949 21.4686 20.7676 20 0 0 0 0 0  
0 0 0 0 0 0 0 0 0 0 0 0 0 0 0 0  
0 0 0  
];  
% R90



0 ;  
 0.001 3.33333 6.66667 10 13.3333 16.6667 20 23.3333 26.6667 30 33.3333 36.6667 40  
 43.3333 46.6667 50 53.3333 56.6667 60 0 0 0 0 0 0 0 0 0 0 0  
 0 0 0 0 0 0 0 0 0 0 0 0 0 0 0 0 ;  
 0.001 3.33333 6.66667 10 13.3333 16.6667 20 23.3333 26.6667 30 33.3333 36.6667 40  
 43.3333 46.6667 50 53.3333 56.6667 60 0 0 0 0 0 0 0 0 0 0 0  
 0 0 0 0 0 0 0 0 0 0 0 0 0 0 0 0  
 ] ;  
 T90 = [414.031 399.427 384.822 369.172 351.424 333.677 317.409 301.894 286.35 269.498  
 254.932 242.095 227.316 213.61 202.25 189.767 177.796 168.022 157.578 147.449 139.24  
 130.608 122.251 115.45 108.404 101.595 96.0103 90.2904 84.7239 79.9203 75.0334  
 70.2837  
 66.1791 62.0283 57.9995 54.5163 51.0146 47.6199 44.683 41.7451 38.9005 36.4392 33.988  
 31.6176 29.568 27.5356 25.5728 23.8783 22.2049 20 ;  
 333.359 322.469 311.58 300.038 287.394 274.75 262.669 250.56 238.653 228.166 216.131  
 203.679 193.933 183.679 172.322 163.637 154.823 145.05 137.425 129.899 121.69 115.243  
 108.898 102.098 96.6714 91.3326 85.7476 81.0533 76.4151 71.6115 67.5666 63.5718  
 59.4672  
 56.0072 52.5918 49.1087 46.1699 43.2704 40.3335 37.8544 35.4095 32.9481 30.8713  
 28.824  
 26.7744 25.0473 23.3456 21.6512 20 0 ;  
 269.044 261.182 253.32 244.734 235.051 225.368 216.799 208.041 199.261 188.821  
 180.599  
 172.52 163.064 155.095 147.752 139.597 132.267 125.698 118.76 112.468 106.851 100.992  
 95.5409 90.5407 85.432 80.7362 76.3615 71.9016 67.8159 64.0079 60.1393 56.6141  
 53.3261  
 49.9966 46.9783 44.1617 41.3179 38.753 36.3587 33.9476 31.7839 29.7643 27.7353  
 25.9238  
 24.2337 22.5394 21.034 20 0 0 ;  
 219.956 213.284 206.613 199.659 192.284 184.909 178.13 171.275 164.421 157.564  
 150.708  
 143.697 137.636 131.202 124.376 118.803 113.23 107.32 102.373 97.4254 92.4129 87.8848  
 83.3567 78.9111 74.8581 70.8052 66.8708 63.2965 59.7222 56.2758 53.1556 50.0355  
 47.0446  
 44.3459 41.6472 39.074 36.7602 34.4463 32.2512 30.2841 28.317 26.4599 24.802 23.1442  
 21.5858 20 0 0 0 0 ;  
 202.534 202.036 196.245 189.956 183.032 177.066 171.282 164.986 158.508 151.82  
 145.552  
 139.818 133.849 127.748 121.805 116.672 111.272 105.872 101.315 96.3919 91.4858  
 87.4478  
 82.9371 78.4711 74.8004 70.7762 66.7849 63.4907 59.9398 56.4214 53.5083 50.4057  
 47.3343  
 44.7872 42.1014 39.4447 37.2398 34.9352 32.6574 30.7669 28.8063 26.87 25.2642 23.6107  
 21.9788 20 0 0 0 0 ;  
 143.074 139.629 136.184 132.418 128.173 123.928 120.047 116.254 112.388 108.223  
 104.058

100.201 96.5326 92.8644 89.0762 85.2743 81.6799 78.2769 74.7447 71.2126 68.0743  
 64.8326  
 61.591 58.7043 55.7413 52.7783 50.2018 47.5337 44.8656 42.585 40.2191 37.8532 35.8466  
 33.7757 31.7049 29.9544 28.1619 26.3693 24.8583 23.3227 21.7872 20 0 0 0 0  
 0 0 0 ;  
 116.561 114.033 111.506 108.678 105.405 102.131 99.1684 96.2822 93.3329 90.1407  
 86.9484  
 83.8969 80.9362 77.9755 74.8981 71.8136 68.8226 66.0296 63.2366 60.3981 57.5535  
 55.0053  
 52.4862 49.9085 47.4617 45.2045 42.8073 40.637 38.5889 36.4275 34.5001 32.679 30.7628  
 29.0612 27.46 25.7835 24.2984 22.9071 21.4577 20.1746 21.7872 20 0 0 0 0  
 0 0 0 ;  
 64.7491 63.3688 61.9884 60.499 58.8473 57.1956 55.6647 54.1632 52.6214 50.9239  
 49.2264  
 47.6263 46.0892 44.5509 42.9003 41.2498 39.6689 38.1875 36.7062 35.1913 33.6688  
 32.1766  
 30.8222 29.4678 28.1259 26.7912 25.466 24.2856 23.1053 21.9474 20 0 0 0 0  
 0 0 0 0 0 0 0 0 0 0 0 ;  
 52.7887 51.682 50.5753 49.3768 48.0415 46.7063 45.4779 44.2755 43.0388 41.6694 40.3  
 39.015 37.7846 36.5532 35.2198 33.8865 32.6123 31.4226 30.2328 29.006 27.7706 26.5663  
 25.475 24.3836 23.29 22.195 21.1127 20 0 0 0 0 0 0 0 0 0  
 0 0 0 0 0 0 0 0 0 ;  
 42.8346 41.9515 41.0684 40.1077 39.0315 37.9552 36.9728 36.0133 35.0245 33.9226  
 32.8207  
 31.7919 30.8103 29.8278 28.7543 27.6809 26.6577 25.7066 24.7554 23.7668 22.7696  
 21.7982  
 20.921 20 0 0 0 0 0 0 0 0 0 0 0 0 0 0  
 0 0 0 0 0 0 ;  
 34.6035 33.8988 33.1941 32.4249 31.5598 30.6946 29.9118 29.149 28.3613 27.4776  
 26.5939  
 25.7733 24.9934 24.2128 23.352 22.4911 21.6728 20.9151 20 0 0 0 0 0 0  
 0 0 0 0 0 0 0 0 0 0 0 0 0 0 0 0  
 0 0 ;  
 27.8303 27.2698 26.7094 26.0955 25.4022 24.7089 24.0875 23.4837 22.8589 22.1529  
 21.447  
 20.7947 20.177 24.2128 23.352 22.4911 21.6728 20.9151 20 0 0 0 0 0 0  
 0 0 0 0 0 0 0 0 0 0 0 0 0 0 0 0  
 0 0  
 ];  
 % R120  
 y120 = [30 40 50 60 64 80 90 120 130 140 150 160 180 ];  
 x120 = [0.001 3.33333 6.66667 10 13.3333 16.6667 20 23.3333 26.6667 30 33.3333  
 36.6667 40 43.3333 46.6667 50 53.3333 56.6667 60 63.3333 66.6667 70 73.3333 76.6667  
 80 83.3333 86.6667 90 93.3333 96.6667 100 103.333 106.667 110 113.333 116.667 120  
 123.333 126.667 130 133.333 136.667 140 143.333 146.667 150 153.333 156.667 160  
 163.333  
 166.667 170 173.333 176.667 180 183.333 186.667 190 193.333 196.667 ;



0.001 3.33333 6.66667 10 13.3333 16.6667 20 23.3333 26.6667 30 33.3333 36.6667 40  
 43.3333 46.6667 50 53.3333 56.6667 60 63.3333 66.6667 70 73.3333 76.6667 80 83.3333  
 86.6667 90 93.3333 96.6667 100 103.333 106.667 110 113.333 116.667 120 0 0 0 0  
 0 0 0 0 0 0 0 0 0 0 0 0 0 0 0 0 ;  
 0.001 3.33333 6.66667 10 13.3333 16.6667 20 23.3333 26.6667 30 33.3333 36.6667 40  
 43.3333 46.6667 50 53.3333 56.6667 60 63.3333 66.6667 70 73.3333 76.6667 80 83.3333  
 86.6667 90 93.3333 96.6667 100 103.333 106.667 110 0 0 0 0 0 0 0 0  
 0 0 0 0 0 0 0 0 0 0 0 0 0 0 ;  
 0.001 3.33333 6.66667 10 13.3333 16.6667 20 23.3333 26.6667 30 33.3333 36.6667 40  
 43.3333 46.6667 50 53.3333 56.6667 60 63.3333 66.6667 70 73.3333 76.6667 80 83.3333  
 86.6667 90 93.3333 96.6667 0 0 0 0 0 0 0 0 0 0 0 0 0 0  
 0 0 0 0 0 0 0 0 0 0 0 0 0 0 ;  
 0.001 3.33333 6.66667 10 13.3333 16.6667 20 23.3333 26.6667 30 33.3333 36.6667 40  
 43.3333 46.6667 50 53.3333 56.6667 60 63.3333 0 0 0 0 0 0 0 0 0 0  
 0 0 0 0 0 0 0 0 0 0 0 0 0 0 0 0 0 0  
 0 0 0 0 0 0 0  
 ];  
 T120 = [472.782 457.154 441.526 424.843 406.044 387.245 370.092 353.777 337.432  
 319.766  
 304.41 290.801 275.229 260.719 248.529 235.203 222.347 211.559 200.089 188.901  
 179.505  
 169.657 160.075 152.04 143.716 135.64 128.872 121.926 115.209 109.605 103.897 98.3328  
 93.4688 88.5443 83.7467 79.5293 75.2802 71.1423 67.4917 63.8281 60.2624 57.11 53.9575  
 50.8911 48.1779 45.4736 42.8454 40.52 38.2097 35.9667 33.9838 32.0202 30.1158 28.435  
 26.7759 25.169 23.7541 22.3623 21.016 20 ;  
 388.261 376.596 364.931 352.618 339.212 325.805 312.965 300.095 287.427 276.184  
 263.381  
 250.152 239.582 228.502 216.314 206.62 196.794 186.006 177.231 168.543 159.147  
 151.497  
 143.946 135.911 129.377 122.933 116.166 110.69 105.298 99.6952 94.9157 90.1893  
 85.3253  
 81.1496 77.0204 72.803 69.1661 65.5698 61.9192 58.762 55.6405 52.4881 49.7577 47.0589  
 44.3457 41.9949 39.6719 37.3466 35.3329 33.3439 31.3611 29.6465 27.9535 26.2728  
 24.8226  
 23.3916 21.9768 20.759 20 0 ;  
 321.124 312.57 304.016 294.732 284.343 273.955 264.651 255.144 245.614 234.416  
 225.354  
 216.43 206.144 197.218 188.872 179.706 171.301 163.62 155.551 148.055 141.21 134.131  
 127.638 121.681 115.567 110.043 104.981 99.8121 95.0154 90.5165 85.944 81.7187  
 77.7459  
 73.7222 70.0173 66.5273 63.0026 59.7677 56.7165 53.6423 50.8299 48.1753 45.506  
 43.0723  
 40.7745 38.4681 36.373 34.395 32.4131 30.6199 28.9278 27.235 25.7103 24.2726 22.8367  
 21.5493 20 0 0 0 ;  
 269.298 261.946 254.594 246.955 238.889 230.822 223.256 215.584 207.912 200.194  
 192.471  
 184.542 177.498 170.073 162.23 155.613 148.996 141.982 135.909 129.835 123.749 118.34

112.931 107.686 103.002 98.3187 93.7335 89.5088 85.284 81.1769 77.4025 73.6281  
69.9785  
66.6313 63.2841 60.0621 57.1125 54.163 51.335 48.7512 46.1675 43.6993 41.4492 39.1991  
37.0573 35.1097 33.162 31.3147 29.6397 27.9647 26.3819 24.9515 23.521 22.1744 20.9617  
20 0 0 0 0 ;  
250.684 250.203 243.747 236.81 229.204 222.47 215.91 208.827 201.557 194.061 186.889  
180.217 173.29 166.22 159.306 153.126 146.669 140.212 134.713 128.668 122.647 117.833  
112.446 107.121 102.863 98.212 93.5914 89.6826 85.4843 81.3176 77.7809 74.0267  
70.3037  
67.1347 63.8026 60.5005 57.6833 54.745 51.8349 49.3481 46.7726 44.2231 42.0429  
39.7987  
37.5785 35.6797 33.7361 31.8144 30.1721 28.4998 26.8473 25.4371 24.0084 22.5973  
21.3953  
20 0 0 0 0 ;  
185.767 181.536 177.305 172.753 167.724 162.695 157.981 153.344 148.629 143.59  
138.551  
133.822 129.282 124.741 120.099 115.446 111.09 107.1 102.975 98.8512 95.1232 91.2696  
87.4161 83.9426 80.3866 76.8306 73.6754 70.4119 67.1484 64.2916 61.331 58.3704  
55.7936  
53.1354 50.4771 48.1681 45.8018 43.4354 41.3827 39.2926 37.2026 35.3918 33.5594  
31.727  
30.1421 28.5475 26.9528 25.5764 24.1991 22.8219 21.6357 20 0 0 0 0 0 0 0  
0 ;  
154.898 151.584 148.27 144.69 140.713 136.735 133.057 129.45 125.77 121.805 117.84  
114.135 110.6 107.064 103.411 99.7519 96.1906 92.8373 89.4841 86.0831 82.6757 79.579  
76.4989 73.3532 70.3466 67.536 64.5706 61.8468 59.2469 56.5182 54.0425 51.6756  
49.1983  
46.957 44.821 42.5949 40.5839 38.6739 36.6919 34.9027 33.2089 31.4588 29.8799 28.3903  
26.8572 25.4753 24.176 22.8438 21.6439 20 0 0 0 0 0 0 0 0 ;  
92.4279 90.6992 88.9706 87.1211 85.0916 83.0621 81.1413 79.2471 77.3073 75.1919  
73.0766  
71.0536 69.0902 67.1255 65.0328 62.94 60.9159 58.99 57.0641 55.0971 53.1206 51.1742  
49.3687 47.5631 45.7683 43.9798 42.2001 40.5734 38.9467 37.3438 35.7642 34.2081  
32.7676  
31.3271 29.928 28.6116 27.2912 26.032 24.8482 23.6507 22.5337 21.4751 20 0 0 0  
0 0 0 0 0 0 0 0 0 0 0 ;  
78.0784 76.6398 75.2011 73.661 71.9699 70.2789 68.6861 67.1173 65.5097 63.7523  
61.9949  
60.3186 58.6947 57.0697 55.3272 53.5846 51.9012 50.3023 48.7034 47.0592 45.4046  
43.7823  
42.2772 40.7722 39.2617 37.7481 36.2486 34.8847 33.5207 32.1682 30.8303 29.4924  
28.284  
27.0815 25.879 24.754 23.6637 22.5735 21.5528 20 0 0 0 0 0 0 0 0  
0 0 0 0 0 0 0 0 0 ;  
65.789 64.5952 63.4013 62.121 60.712 59.3029 57.9826 56.684 55.352 53.891 52.4299  
51.0407 49.6979 48.354 46.9038 45.4537 44.0549 42.7298 41.4047 40.0336 38.652 37.2981

36.0452 34.7924 33.5306 32.2634 30.9987 29.8587 28.7187 27.5847 26.4596 25.3345  
24.3027  
23.3083 22.3101 21.3039 20 0 0 0 0 0 0 0 0 0 0 0 0 0  
0 0 0 0 0 0 0 ;  
55.2912 54.3 53.3088 52.2443 51.0708 49.8972 48.8041 47.7306 46.6282 45.4142 44.2002  
43.0501 41.9412 40.8314 39.6261 38.4208 37.2605 36.1647 35.0688 33.9281 32.7771  
31.6502  
30.6108 29.5714 28.5195 27.4597 26.402 25.4524 24.5029 23.5563 22.614 21.6716 20.8153  
20  
0 0 0 0 0 ;  
46.3425 45.521 44.6995 43.8158 42.8395 41.8632 40.9597 40.0741 39.1633 38.1561  
37.1488  
36.1983 35.2846 34.37 33.3702 32.3703 31.41 30.5063 29.6025 28.6561 27.6999 26.7646  
25.9055 25.0463 24.1728 23.2904 22.4097 21.6228 20.8359 20 0 0 0 0 0 0  
0  
0 ;  
32.3115 31.7536 31.1957 30.592 29.9204 29.2487 28.6362 28.0381 27.4213 26.7321  
26.0429  
25.3987 24.7836 24.1677 23.4849 22.8021 22.1496 21.5405 20.9314 20 0 0 0 0  
0  
0 0 0 0 0 0 0 0 0 0 0  
];

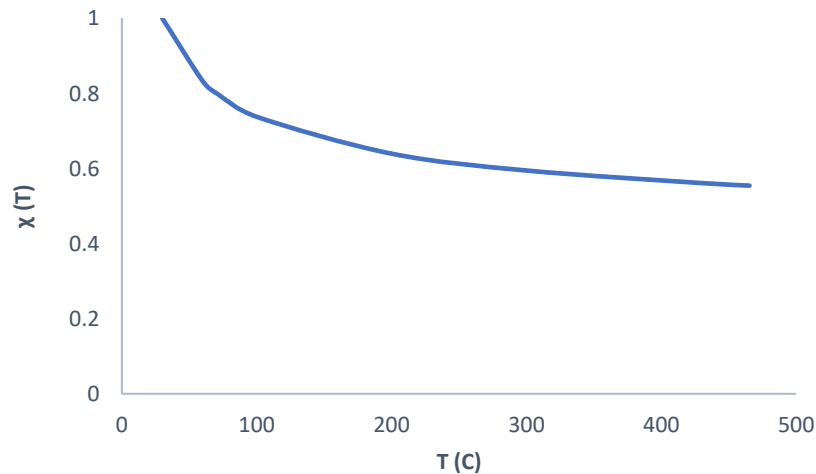
## Annex-C (Example Calculation)

### Given Data:

diameter	<b>d</b>	=	12	mm								
reduc. factor	<b><math>\chi_i</math></b>	=	[	1	0.8	0.8	0.74	0.6	0.6	0.56	0.55	]
Temp.	<b>T</b>	=	[	30	60	71.2	100	200	300	432	465	]
Exp. Time	<b>R</b>	=	120	min								
conc. Cover	<b>y</b>	=	30	mm								
Bond strength	<b>fbd</b>	=	2.7	Mpa								

### Solution:

reduction curve for precast  
side case:

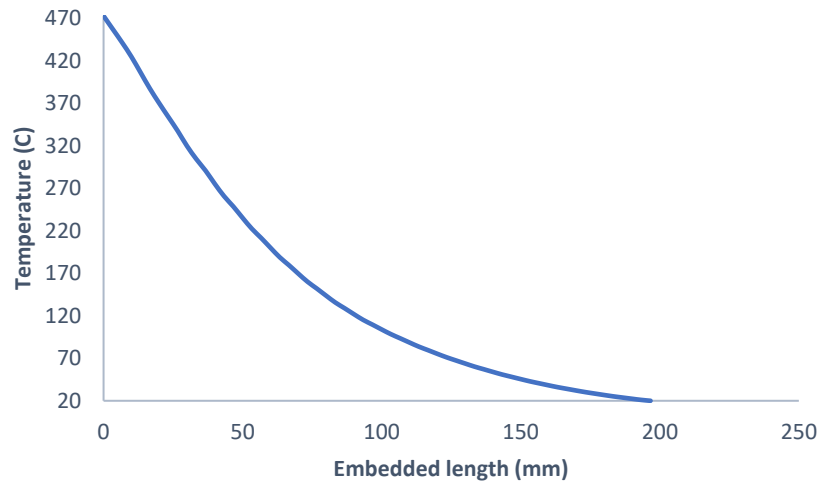


$$\chi(T) = 2.862 \times T^{-0.4436} + 0.3671 \quad 30^\circ\text{C} \leq T \leq 465^\circ\text{C}$$

Note that this equation is a best fit for this (pre-cast side) case within the temperature range of 465 C. For value of temperature higher than 465 C reduction factor is equal to zero.

Temperature profile is extracted from heat transfer analysis of a beam column connection.

Temperature profile for 120 minute of exposure time at 30 mm concrete cover:



$$T(x) = 495.6 \times e^{-0.01359 \times x} \quad 0 \text{ mm} \leq x \leq 196.67 \text{ mm}$$

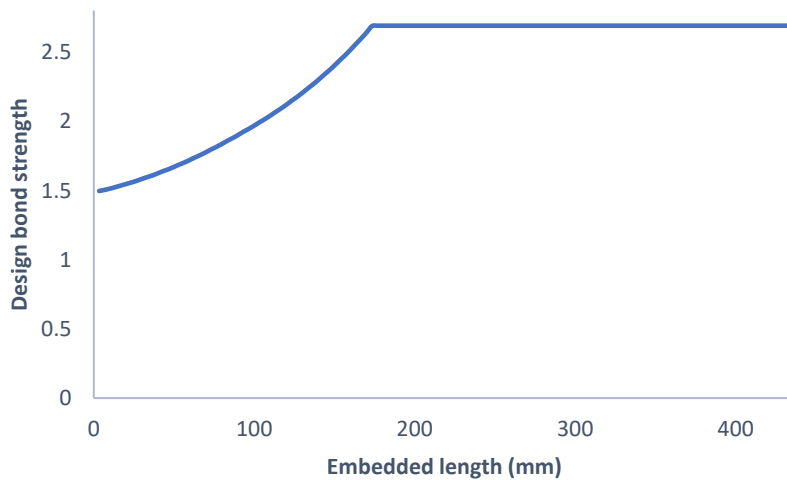
\*\*Note that this equation is for concrete cover of 30 mm.

Basic Anchorage length at ambient temp. :

$$L_{d,20C} = \frac{\emptyset}{4} \times \frac{f_{yd}}{f_{bd,20C}} = 436 \text{ mm}$$

Now that we have  $\chi(T)$  and  $T(x)$ , we can get  $\chi(T(x))$

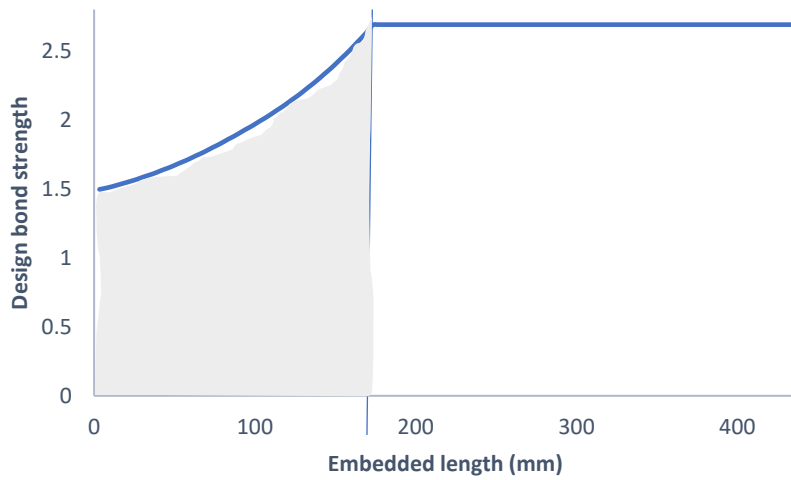
reduced bond strength can be computed as :  $f_{bd,T(x)} = \chi_{T(x)} \times f_{bd,20C} \frac{Y_m}{Y_{m,fi}}$



$$f_{bd,T(x)} = 0.0001985 \times x^{1.679} + 1.519 \quad 0 \text{ mm} \leq x \leq 173.33 \text{ mm}$$

Note that this equation represents only temperature affected part of bond strength, which in this case extends for the embedded length from 0 to 173.33 mm. Now to find the amount of bond strength lost during fire exposure and the scheme to accommodate it is as follows:

Area under the curve is :  $\int_0^{173.33} f_{bd,T(x)} dx = 337.03 \text{ N/mm}$



The amount of bond strength lost is : A =

$$\left\{ (f_{bd,20C} \times (173.33 - 3.33)) - 337.032 \right\} + (f_{bd,20C} \times 3.33)$$

$$= 129.23 \text{ N/mm}^2$$

The increment in length to accommodate strength loss is :

$$\Delta L \times f_{bd,20C} = A \rightarrow \Delta L = \frac{A}{f_{bd,20C}} = 48.04 \text{ mm}$$

Then the incremented length is :

$$L_{d,T} = \Delta L + L_{bd,20C} = 486.41 \text{ mm}$$

Thus the amplification factor  
is :

$$\alpha = \frac{L_{d,T}}{L_{bd,20C}} = 1.12$$